INVITED PAPER

Mott Memory and Neuromorphic Devices

Correlations of electrons—arising in structural and physical phase transitions—provide a nanoscale-compatible mechanism of possible utility to electronics. This paper discusses the mechanisms and their implications in memory and information processing.

By You Zhou and Shriram Ramanathan

ABSTRACT | Orbital occupancy control in correlated oxides allows the realization of new electronic phases and collective state switching under external stimuli. The resultant structural and electronic phase transitions provide an elegant way to encode, store, and process information. In this review, we examine the utilization of Mott metal-to-insulator transitions, for memory and neuromorphic devices. We emphasize the overarching electron–phonon coupling and electron–electron interaction-driven transition mechanisms and kinetics, which renders a general description of Mott memories from aspects such as nonvolatility, sensing scheme, read/write speed, and switching energy. Various memory and neuromorphic device architectures incorporating phase transition elements are reviewed, focusing on their operational principles. The role of Peierls distortions and crystal symmetry changes during phase change is discussed. Prospects for such orbitronic devices as hardware components for information technologies are summarized.

KEYWORDS | Complex oxide; emerging memory; metal oxide; metal-to-insulator transition; Mott insulator; neuromorphics; nonvolatile; orbitronics

I. INTRODUCTION

The scaling of semiconductor devices approaching 10-nm critical dimensions is much indebted to the success of the electronic band theory. Nevertheless, as early as 1937, de Boer and Verwey noted that the band theory is insufficient to explain the electrical properties of many transition metal oxides with a partially filled *d*-electron band, which were expected to be metallic but are insulators in reality [1]. In 1949, Mott put forward a theory on how electron–electron interactions in these materials (commonly referred to as Mott insulators despite the fact that many of them display complex electronic phase diagrams that may not be wholly described by the original theory) could explain their insulating states [2]. It was later discovered that Mott insulators not only show unconventional electrical insulating behavior, but also often exhibit interesting phase transitions with drastic change in their electrical and magnetic properties under various stimuli. In the words of Nevill Mott, the Mott transition can strictly be defined as a "transition from an antiferromagnetic insulator to a metal" [3]. In this review, we use the terminology of Mott materials in a broader sense to describe materials with strong correlation that show insulator-to-metal transitions despite the fact that ordering of spins may not exactly coincide with electrical conductivity changes.

Recently, the potential applications of Mott insulators, especially those manifesting metal-to-insulator transitions, in memory devices have been actively explored, as the phase transitions could be triggered at subnanosecond timescales [4], [5] and the state of devices can be accessed electrically. It is also noteworthy that the electronic-structural phase changes in complex oxide thin films are robust and reversible for millions of cycles, in sharp contrast to bulk single crystals that shatter across the transition due to stress buildup. The enhanced reliability of phase transitions has contributed to the exponential growth of interest in this topic from not only applications' point of view but also the ability to study intrinsic physics of the transition with low-dimensional materials. In turn, this motivates state-of-the-art experimental techniques such as ultrafast diffraction, spectroscopy and other *in situ* diagnostics to be applied to

Manuscript received September 28, 2014; revised April 1, 2015; accepted May 6, 2015. Date of publication June 26, 2015; date of current version July 15, 2015. This work was supported by the Army Research Office under Grant W911NF-14-1-0669; by the Air Force Office of Scientific Research under Grant FA9550-12-1-0189; and by the National Academy of Sciences.

The authors are with the John A. Paulson School of Engineering and Applied Sciences, Harvard University, Cambridge, MA 02138 USA (e-mail: youzhou@seas.harvard.edu; shriram@seas.harvard.edu).

Digital Object Identifier: 10.1109/JPROC.2015.2431914

0018-9219 © 2015 IEEE. Personal use is permitted, but republication/redistribution requires IEEE permission.
See http://www.ieee.org/publications_standards/publications/rights/index.html for more information.

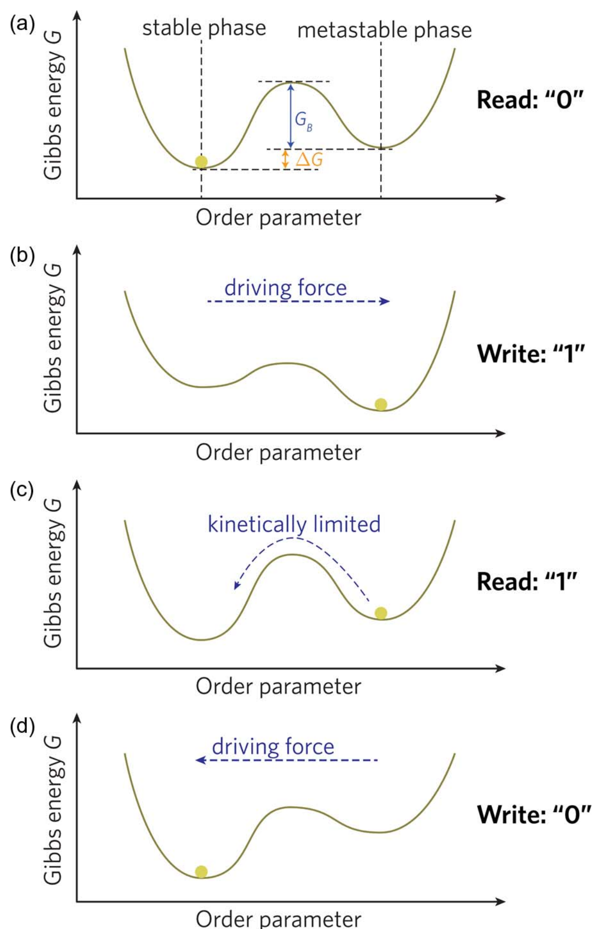

Fig. 1. ***Free energy landscape of Mott memories under writing and reading signals as a function of order parameter. (a) At the standby temperature, the system at equilibrium is in its thermodynamic stable phase (state "0"). ΔG is the free energy difference between stable and metastable phases (state "1"). (b) An external stimulus drives the phase transition from state "0" to state "1" and the minimum energy cost and the minimum energy dissipated in the system is ΔG. (c) When the writing signal is removed, the system in state "1" faces an energy barrier of G_B and the relaxation to state "1" is limited by the kinetics of the transition. The relative magnitude of kinetic barrier G_B and thermodynamic driving force ΔG determines whether the state is volatile. The memory is volatile if the metastable state "1" cannot be retained for a significant period of time. Otherwise, it can function as a nonvolatile memory and (d) another external signal is needed to change "1" back to "0."***

such problems, furthering our fundamental understanding of strong correlations in complex systems.

The general idea of utilizing Mott transition in memory devices is illustrated in Fig. 1 by considering the Gibbs free energy landscape of the system under write and read signals. Initially, the system is in the stable phase (state "0"). An external stimulus drives the phase transition from the thermodynamically stable phase to the metastable phase (state "1") (for example, from the insulating state to the metallic state). When the stimulus is removed, the relaxation to state "0" is limited by the kinetics of the phase transition. If the kinetic barrier is much smaller than the thermodynamic driving force, the metastable state "1" could not be retained for significant period of time and the memory will be mono-stable and volatile. With a large kinetic barrier, on the other hand, the device would be quasi-bistable and nonvolatile, in which case another external stimuli is needed to switch from "1" to "0." Theoretically, it is even possible to realize both volatile and nonvolatile operations with a single material at two different temperatures with different magnitude of thermodynamic driving force. By way of illustration, many of the phase transitions of Mott insulators are hysteretic at temperatures close to T_c, which could enable the nonvolatile operation. On the contrary, the stable phase will always be restored in the absence of external stimuli if the ambient temperature is outside the hysteretic window.

In comparison with memory devices like DRAM and SRAM, where the state is stored in the form of charge on capacitors, the state of Mott memories could be memorized and read out in the form of electronic and magnetic properties. This enables the compact packing of two-terminal cross-point array with $4F^2$ cell area size (F is the minimum chip feature size). What is more, the speed of electrically triggered Mott transitions [6], [7] in two-terminal devices is comparable with standard memory devices including DRAM, SRAM, and faster than Flash [8], while the demonstrated speed of optically triggered switching can even approach the gate delay of the state-of-the-art transistors [9]. It has also been demonstrated that the write energy per transition is sub-100 fJ and could be scaled down with smaller device dimensions [7]. Additionally the write/read voltage values are compatible with typical supply voltages of silicon circuits.

The outline of the paper is as follows. Section II overviews the Mott transition phenomena and introduces the key mechanisms involving cooperative structural and electronic phase change to the general reader. Various devices that have been realized to date utilizing Mott transitions for memory and neuromorphic devices are discussed in Section III. Section IV evaluates and benchmarks the performance metrics of Mott transition memory devices, followed by a summary section.

II. MATERIAL PROPERTIES

A. Metal-to-Insulator Transition Phenomena

Several types of phase transitions involving change in magnetic, electric, and mechanical properties exist in the family of Mott insulators. The metal-to-insulator transitions refer to a class where the competition between the electron localization and delocalization lead to drastic changes in the conductivity of materials. These phase transitions can be triggered by thermal energy, electric fields, and optical stimuli, and the state of the system can be

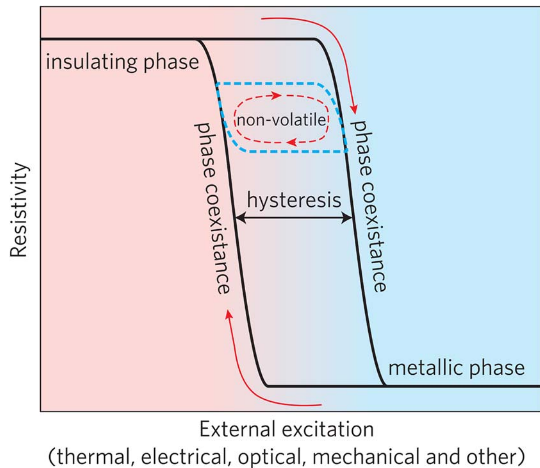

Fig. 2. ***Generic features of metal-to-insulator transitions. The metal-to-insulator transition in Mott insulators can be driven by various kinds of external perturbations. Above a threshold perturbation, the material resistivity changes drastically by several orders of magnitude. Near the threshold, phase coexistence of both insulating and metallic phase can occur. Many of the transitions also exhibit hysteresis. Within the hysteresis window, the system's resistance could be nonvolatile.***

readily read out by electrical or magnetic signals. Fig. 2 illustrates some of the generic features of how the resistivity of the materials responds to external perturbations. 1) The system is initially in the insulating phase. As the external perturbation reaches a certain threshold value, a sharp phase transition is induced and the resistance drops by several orders of magnitude. When the external perturbation is removed, the system reverts back to the insulating phase. 2) The intermediate state between the insulator and metal is the coexistence of both phases [10]–[12], usually reflected by the sharp yet smooth change in resistivity as a function of perturbation. Transitions with no phase coexistence may be observed when the size of the device is smaller than the domain sizes. 3) Many transitions are hysteretic, meaning the perturbation strength to induce phase transition in one way is different from that in the other way. 4) Within the hysteresis window, the resistivity value depends on not only external field but also history and could be nonvolatile (dashed line and arrows in Fig. 2).

B. Elementary Mott Transition Mechanisms

In classical band theory, electrons could be treated as particles that move in an effective periodic potential independently from other electrons. Band forms from the overlapping atomic orbitals and the bandwidth W is related to the system's energy gain from electron delocalization, or equivalently electron's kinetic energy that is often denoted as t. Materials with partially filled orbitals also have partially filled bands and are therefore metals. This criterion fails for Mott insulators, such as transition metal oxides with partially filled $3d$, $4d$, or $4f$ orbitals. In such materials, the Coulomb repulsion energy between electrons (electron correlation), often being referred to as U, is stronger than the kinetic energy t and can therefore inhibit electrons from delocalizing to form bands or hopping through the lattice [Fig. 3(a)]. In the band picture, the original partially filled electronic band splits into one empty band and one filled band. The material is hence insulating.

The competition between carrier localization and delocalization drives the transition between insulating and metallic states. One way to induce such a phase transition is to tune the magnitude of delocalization energy t or, in other words, the bandwidth W. For example, compressing the lattice constant by external stress can increase W and leads to bandwidth-controlled MIT, as illustrated in Fig. 3(b). The other way is to change the effective U between

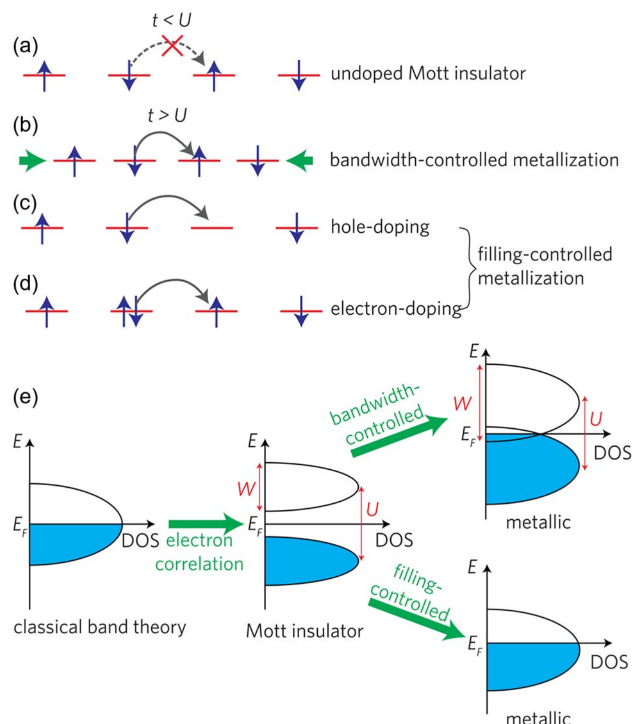

Fig. 3. ***Mechanisms of metal-to-insulator transitions in Mott insulators. (a) In the insulating phase, electron transport/hopping is forbidden because Coulomb repulsion between electrons U is much larger than electron's kinetic energy t. (b) Bandwidth-controlled metal-to-insulator transition: decreasing the interatomic distance increases the electronic bandwidth and delocalization energy t and drives an insulator-to-metal transition when t becomes larger than U. (c) and (d) Filling controlled metal-to-insulator transition: hole- and electron-doping create empty or doubly occupied atomic sites, respectively. Since there is no more energy penalty for electron hopping to occur, the insulator becomes a metal. (e) The electronic band diagram evolution during metal-to-insulator transitions: classical band theory predicts that a Mott insulator has nonzero density of states at the Fermi level and is metallic. In reality, the band splits into two as a result of electron correlation and Fermi energy lies in the gap. Both increasing the bandwidth W and introducing extra carriers can lead to the collapse of the bandgap.***

electrons. When electrons/holes are added into the system, the energy cost for hopping is reduced for certain electrons, reducing the effective Coulomb repulsion energy U [Fig. 3(c) and (d)]. This can be also seen from the perspective that the added carriers can more effectively screen the electron–electron interaction and reduce U. The carrier-induced transition is referred to as filling-controlled MIT. In some cases, both mechanisms may come into play, e.g., certain temperature-driven transitions. The evolution of band structure across bandwidth-controlled and filling-controlled MITs is shown in Fig. 3(e).

C. Interplay Between Various Degrees of Freedom

The so-called Mott transition is purely electronic and does not take other interactions into account. An important feature of Mott insulators in reality, however, is that the energy of many other interactions is on the same order of magnitude with electron–electron correlation U and kinetic energy t, and therefore these interactions also become relevant in accurately dictating a material's electronic properties. These include electron–lattice, spin–spin, and other types of interactions. As a result, although intrinsic Mott transitions should be purely electronic in origin and not assisted by lattice, charge, and other degrees of freedom, the interplay between them leads to the observation that most of the electronic phase transitions in transition metal oxides are accompanied by structural and other types of transition. It is also important to note here that the structural symmetry changes might initiate electronic transitions or *vice versa*, so these can be inherently coupled. In this section, we consider examples where the interplay between different degrees of freedom is important in studying the MIT properties.

Since d orbitals are degenerate [fivefold degenerate in spherical potential, and split into two levels in a tetrahedral or octahedral crystal field because of broken symmetry: e_g level with twofold and t_{2g} level with threefold degeneracy, as shown in Fig. 4(a)], the localized d electrons can occupy multiple possible orbitals, adding an orbital degree of freedom to the system. In addition, crystal structural change (the lattice degree of freedom) modifies the electronic band structure, which could be coupled with Mott transitions. For example, Fig. 4(b) shows how the elongation of metal-oxygen bonds along the z-axis of the MO_6 octahedron, i.e., Jahn–Teller effect, can lift the degeneracy in e_g and t_{2g} levels, which could lead to metal-to-insulator transitions for certain electron configurations [13]. In oxides with rutile structure, the interaction between metal ions in the edge-sharing MO_6 octahedra also modifies the band structures, as shown in Fig. 4(c). The $d_{//}$ orbital has electron lobes pointing along the rutile c-axis, whereas the π^* orbitals have their electron lobes in the plane perpendicular to the c-axis. This unique aspect of band structure lays the foundation for the MIT in VO_2, as will be discussed in detail in Section II-D.

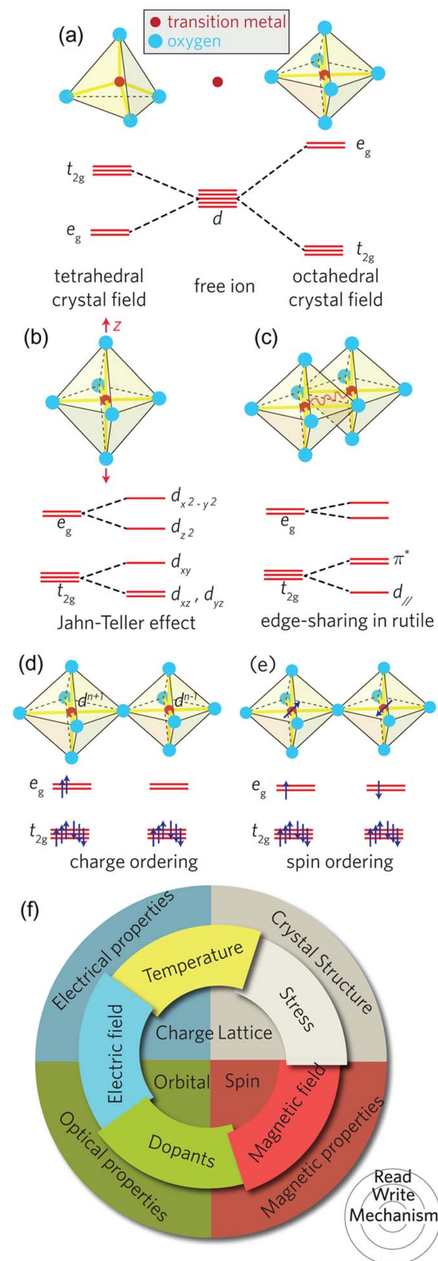

Fig. 4. *Interplay between various degrees of freedom in Mott insulators. (a) Crystal field splits the originally fivefold degenerate d-orbitals into a twofold degenerate e_g and a threefold degenerate t_{2g}. The relative energy of e_g and t_{2g} levels depends on the coordination number of the metal ion. (b) Jahn–Teller effect (elongation of M–O bond along the z-axis of the octahedron) and (c) metal-to-metal interaction in rutile (examples include TiO_2 and the metallic state of VO_2 and NbO_2) can both further lift the degeneracy of e_g and t_{2g} levels and modify the band structure. (d) Charge ordering and (e) spin ordering can also occur and influence the transport properties of correlated oxides. (f) In Mott insulators, different degrees of freedom are coupled together, making them sensitive to various perturbations and showing changes in different physical properties. The inner circle shows the coupling between various degrees of freedom. The mid-ring represents various ways to trigger phase transitions and the outer ring illustrates the physical properties that can be changed by the transitions.*

In addition to the lattice degree of freedom, long-range charge or spin ordering can also occur (charge and spin degrees of freedom). Fig. 4(d) and (e) gives examples of charge ordering and spin ordering in oxides with d^7 electron configurations. Charge ordering can lead to spatially varying metal–oxygen bond length and insulating electrical properties. A well-known example is the MIT in magnetite Fe_3O_4 discovered by Verwey [14]. It is also believed that charge-ordering plays an important role in the MIT of the rare earth nickelates [15]. Similarly, spin ordering also influences their electronic transport behavior, and is very often a natural result of charge localization. From the above discussion, it can be seen that the charge, lattice, spin, and orbital degrees of freedom are coupled in Mott insulators, which gives rise to complex phase diagrams [16]–[18]. For the same reason, the mechanisms of many phase transitions may be better explained by the cooperations between various interactions, rather than one single driving force [19].

The competition between different degrees of freedom enables one to trigger the transition by various means, as shown in Fig. 4(f), which allows flexibility in the operational principles of the Mott insulator devices. Similarly, the phase transitions can be reflected in change of different physical properties and therefore could be sensed with electrical, magnetic, or optical probes. For example, external magnetic fields can lead to large changes in the resistivity of some oxides, which is often called colossal magnetoresistance [20]. On the other hand, it is also possible to use an electric field to control the magnetization in the materials, also known as magnetoelectric effect [21], [22], which can be of interest in signal transduction or read out. Some Mott insulators exhibit ferroelectric properties, and can thus be integrated into the gate stack of conventional transistors for capacitance enhancement [23] or as a state register in memory. Because of the electron–phonon interaction, external stresses can also trigger changes in electronic/magnetic properties, which can be used as sensors for instance or mechanical energy harvesting or storage. Among the many methods to induce and sense the transitions, perhaps the most direct operation manner of a Mott-insulator-based memory device is to drive both the metal-to-insulator transition and sense the device conductance electrically. Yet the diversity of the MIT writing/reading methods may add new functionalities to conventional memory technologies. The field of orbitronics explores such devices utilizing the orbital occupancy control in various materials.

D. VO_2: A Case Study

In this section, we examine a classical MIT material VO_2, as an example to show how the lattice degree of freedom is coupled to the Mott transition. VO_2 exhibits an insulator-to-metal transition accompanied by a structural transition with a transition temperature of ~67 °C. The proximity to room temperature allows in-depth studies into the transition mechanism by a plethora of experimental techniques advanced in the past two decades. In contrast, NbO_2 that undergoes insulator-to-metal transition at nearly 1083 K is far less studied and presents a formidable challenge. Simply retaining the phase and preventing oxidation to the more stable 5+ valence of Nb at the thermal transition is a daunting problem. This compositional complexity will be discussed in Section II-G.

In its metallic phase, VO_2 has a rutile structure (the so-called R phase), and the $d_{//}$ and π^* orbitals form two overlapping electronic bands, as shown in Fig. 5(a). If there are totally N vanadium atoms, there are N d electrons

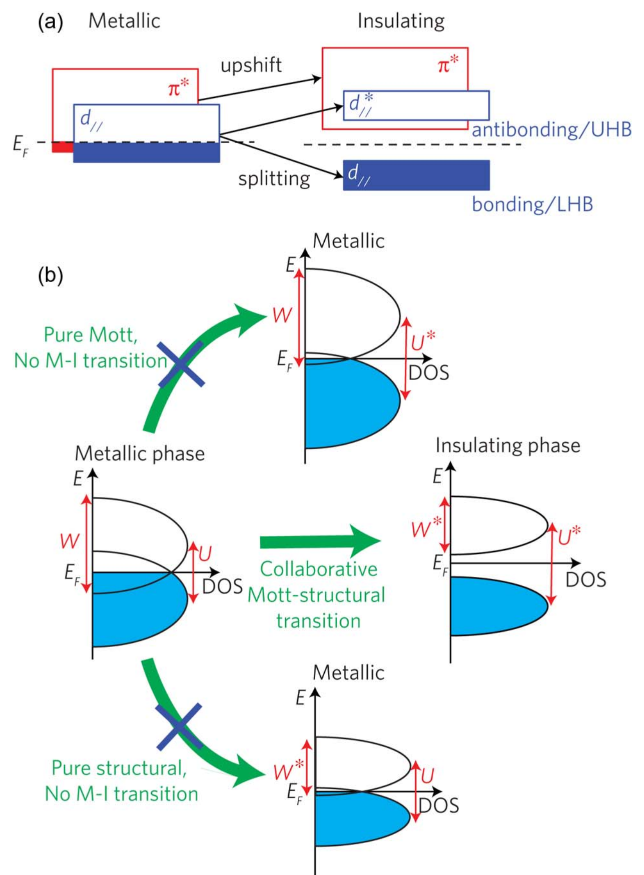

Fig. 5. *Cooperative lattice and electronic phase change in correlated insulators. (a) Band structure of metallic R phase and insulating M1 phase VO_2. In the metallic phase, $d_{//}$ and π^* bands overlap with each other and both are partially filled. In the Goodenough picture (or Pierels picture), the dimerization of V atoms splits $d_{//}$ band into bonding and antibonding state and tilt of the dimers upshifts π^* band. In the Mott picture, π^* band is upshifted and depopulated from structural change, leading to less screened electron correlation and splits $d_{//}$ band into UHB and LHB. (b) Illustration of collaborative Mott-structural transition. A Mott transition reduces effective electron correlation U, but may not be enough to induce a metal-to-insulator transition. The decrease of bandwidth W from structural change alone may also be insufficient to trigger the transition. A simultaneous increase in U and a decrease in W can drive the transition in a collaborative fashion.*

and the total density of states in the overlapped band is 6N. The material is thus a metal. Across the electronic metal-to-insulator transition, VO_2 changes into a monoclinic structure characterized by vanadium dimerization and tilt of the dimers along the rutile c-axis (named M1 phase). In the Goodenough picture, the dimerization of V–V pairs splits the $d_{//}$ state into a bonding state and an antibonding state [24]. At the same time, the tilt of V dimers upshifts the π^* bands. The combined structural change lifts the degeneracy and leads to a metal-to-insulator transition in Fig. 5(a). This picture is based solely on band theory and does not consider any electron correlation effect and often called Peierls transition. On the other hand, Zylbersztejn and Mott attributed the MIT mechanism to electron correlation [25]. They argued that the bandgap ($\sim$0.6 eV) cannot be quantitatively described by the Goodenough picture without taking into account the Hubbard U. In the Mott picture, the structural transition upshifts and depopulates the π^* bands, making the electron repulsion on the $d_{//}$ band less screened by the free carriers. The lower density of free electrons thus splits $d_{//}$ band into the upper and lower Hubbard bands (UHB and LHB) and triggers the transition. Note that even in Mott's original picture, the structural transition is an important factor in explaining the transition [25]. For the past few decades, the nature of the MIT in VO_2 has been heavily discussed [25]–[30]. Later observations of another monoclinic insulating phase (M2 phase) under doping and stress have further complicated the interpretation [31], [32]. Many recent studies point to a combined effect of lattice distortion and Coulomb correlation [30], [33]–[39], since neither Mott nor Peierls mechanism could alone explain the wide range of phenomena in VO_2.

The phase transition dynamics studies reveal important knowledge on the following questions: Does the electronic transition happen before the structural transition? It has been found that the transition from initial insulating to the stable metallic state can be mediated through a metastable metallic phase [40]. This intermediate phase is structurally different from both the normal metallic and insulating phases. It is characterized by local atomic motion and the dilation of the vanadium–vanadium bond. The intermediate phase finally transits into the stable rutile phase. This shows that the electronic transition can happen before the full structural transitions, yet still coupled partly to it. To what degree can the electronic and structural transition be decoupled? Is it possible to achieve and also reverse the MIT without structural changes in VO_2? There are several studies suggesting that there is a monoclinic metallic phase [41]–[48], which points to the possibilities of pure electronic transitions. The transitions could have different trajectories in phase space depending upon the experimental conditions and driving force. Some of the observations were made under nonequilibrium conditions [49] or with multiple driving forces, such as in thermally triggered MIT of strained VO_2 [42], [46], [47]. The nature of the monoclinic metallic phase, however, also needs to be carefully studied. Most X-ray diffraction studies only monitor the out-of-plane lattice constant change, and therefore do not provide full information on the whole crystal structure. Future works studying the entire reciprocal space could help to resolve the issue of whether there is absolutely no structural change and an intrinsic pure Mott transition can be induced in VO_2 by various driving forces. In addition, the interpretation of experimental results is complicated by phase coexistence [10], [50], a generic feature of first-order phase transitions, near the transition temperature. Using X-ray diffraction mapping, it has been shown that only low-temperature monoclinic and high-temperature tetragonal phases exist at the transition temperature, and there is no evidence for the presence of V dimers above the transition temperature in the thermally driven transition [51].

Fig. 5(b) illustrates the generic idea of a Mott transition coupled with a structural transition. In the metallic phase, the electron correlation energy corresponds to an effective Coulomb repulsion U that is screened by the free electrons. The bandwidth W is determined by the structure. In a pure Mott transition, the electron correlation energy increases, for example, by freezing out the free carriers by cooling. If bandwidth W is, however, still larger than the unscreened Hubbard U^*, the MIT cannot be induced solely by electron correlation. On the other hand, a structural change can reduce the bandwidth to a lower value W^*, but may also not induce an MIT unless U is small. By combining both effects, i.e., reduction of bandwidth and increase in the correlation, it then becomes possible to open up a bandgap and create an insulating phase. Of course, this picture does not provide a universal description of all the MIT phenomena. As discussed, a Mott transition in reality could be accompanied by symmetry breaking or change in the other degrees of freedom as well, and the structural change does not only modify bandwidth W, but also the band's relative position to the Fermi level. Therefore, each material may require specific detailed investigations. Suppose that if an external driving force such as strain is used to mimic the role of structural change (e.g., to modify the bandwidth), it then becomes possible to induce a pure Mott transition without the help of structural transition. This presents a promising route to explore purely electronic transitions, and the use of low-dimensional materials can contribute to advancing this frontier.

E. Surface Versus Bulk Effects

Surfaces of transition metal oxides can display properties distinct from bulk [52]. First, because of the net charges on the cation and oxygen anion, the surface of the crystal can exhibit a dipole, which is referred to as a polar surface. Polar surfaces are in general less stable than nonpolar surfaces and usually go through reconstruction to compensate the dipole moment. Second, the degree of coordination is unsaturated for the surface ions. Dangling bonds could interact with molecules in the environment if

the surface is exposed. The unsaturation and dangling bonds will change the orbital thermodynamics in Fig. 4(a) and could lead to different electronic structure at the surface from the bulk. Third, as defects such as oxygen vacancies are more likely to form on the surface, they will also change the surface of the electronic structure. The scaling of the metal-to-insulator transitions discussed in this review can be imposed by the feasibility of retaining the same crystal structure in lower dimensions as the bulk. When scaling down the material, the total Gibbs free energy will be dominated by the surface rather than the bulk energy. As a result, the thermodynamically stable phase for low-dimensional oxides can be different from the bulk. All of the above surface effects could be coupled to other degrees of freedom, leading to emergent surface properties, although the fundamental physics is unchanged.

For VO_2, it has been noted that both the insulating and metallic phases as well as the transition mechanism remains the same as the bulk for thin films down to ~4 nm, which suggests VO_2 can be scaled down to such sizes without losing the functionality arising from phase change [53]. In VO_2 nanowires, it has been observed that the VO_2 surface stress can stabilize M2 phase [54], although the question whether there will be fundamentally different phase at the surface from the bulk remains to be explored. Another example is the observation of a pure Mott transition without structural change at $Ca_{2-x}Sr_xRuO_4$ surface [55]. In the low Sr doping regime, bulk $Ca_{2-x}Sr_xRuO_4$ exhibits a metal-to-insulator transition and a concomitant structural change at ~154 K with a Mott insulating ground state. It has been demonstrated that the structural distortion is important to create and stabilize the Mott insulating state in the bulk [56]–[58]. By studying the electrical properties and crystal structures of $Ca_{2-x}Sr_xRuO_4$ ($x = 0.1$) surface, it was shown that the surface of the material goes through MIT at lower temperature (~130 K) and there is no related structure change [55]. It is found that the surface RuO_6 octahedra have larger rotational distortion and tilt than the bulk parts, which helps to narrow the t_{2g} bandwidth. Presumably these effects increase the ratio of Coulomb U to bandwidth W, enabling the Mott transition without structural change.

On the other extreme, growing thick films of phase change materials approaching a micrometer or more remains a challenge due to the slow growth rates and retaining the single phase or stoichiometry. Self-annealing during the long growth cycles can lead to through-thickness compositional changes. Such thick films are gaining importance in the field of nonlinear optical materials and optical limiters and will require much effort in synthesis.

F. Electrically Triggered Metal-to-Insulator Transition

Fig. 6(a) shows typical current–voltage curves of E-MITs in two-terminal Mott metal–oxide–metal devices (e.g., VO_2 [59], V_2O_3 [60], NbO_2 [7], manganites [61], magnetites [62], and $La_{2-x}Sr_xNiO_4$ [63]). In the low-voltage region, the device shows linear I–V curve as in its insulating phase. Under large bias, the I–V curve begins to deviate from linearity and above a certain threshold voltage V_{th}, the device resistance drops drastically. The corresponding threshold electric field is typically 10^4–10^5 V/cm [6], [7], [59], [60], [64]. The I–V curve becomes linear again well above V_{th}, and the device is switched ON. When voltage is ramped down, the device turns OFF at V^*_{th} that is smaller than V_{th}, showing a hysteresis in the I–V curve. Such switching behavior is often referred to as "threshold

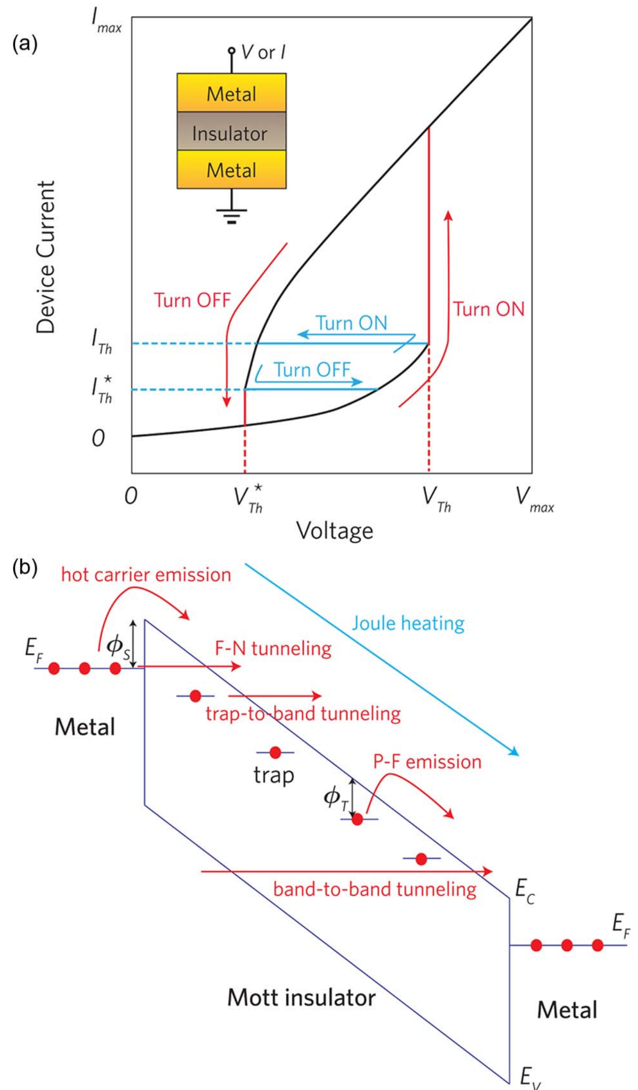

Fig. 6. *(a) Typical current–voltage curves of electrically triggered metal-to-insulator transitions either driven by voltage or current source. (b) Possible mechanisms of the electrically triggered transition include: thermal Joule heating, and carrier injection due to Schottky thermionic emission, Fowler–Nordheim tunneling, Poole–Frenkel emission, trap-to-band tunneling, and band-to-band tunneling. Some of the processes require formation of Schottky barriers or presence of trap states.*

switching." In addition to voltage triggering, E-MIT can be also driven by a current source, which exhibits current-controlled negative differential resistance (CC–NDR) phenomena near the threshold current I_{th}, as shown in Fig. 6(a) [65], [66]. In a symmetric device, the I–V curve is independent of the voltage polarity. The threshold switching is due to metal-to-insulator transition and not defect-related conductive filament formation as in RRAM based on the following observations: 1) the ON/OFF ratio of E-MIT matches the transition magnitude of thermal MIT [67]; and 2) the ON/OFF resistance scales with the device area [6]. Both suggest bulk MIT instead of defect-related conductive filament (CF) formations [68]. Note that sometimes there will be multiple jumps in the I–V curves, due to partial switching in multiple domains [67], [69]–[71]. The cross section of such conductive path is usually on the order of micrometers to millimeters and comparable with the device area [70], [71], in sharp contrast to the nanoscale CFs in RRAMs. Additionally, two terminal Mott switches could also be multileveled when taking advantage of the hysteresis of the transitions [72]. In samples synthesized with structural and compositional disorder, it is indeed possible to form local switching mediated by point defects that show bipolar switching behavior [73], [74]. The E-MIT is also different from that of phase change random access memories (PCRAMs). In PCRAMs, resistive switching is achieved by switching between amorphous and polycrystalline phases such as in chalcogenides [75], [76].

Several mechanisms could be responsible for inducing E-MITs, as illustrated in Fig. 6(b). First, Joule heating as a result of the current passed through can elevate the device temperature and drives MIT. Additionally, since the change in the carrier density can also cause a Mott transition by filling control, any process that introduces extra carriers in the conduction/valence band may also induce E-MIT. Such effects include: 1) Fowler–Nordheim tunneling through or thermionic emission across a Schottky barrier if the metal/insulator contact is non-Ohmic [77]; 2) Poole–Frenkel emission or trap-to-band tunneling in presence of defect states [78]–[80]; and 3) band-to-band tunneling, etc. It has been argued that Joule heating could not alone cause the transition [81]–[83], and the nonlinearity of I–V curves just below V_{th} could also be a signature of Poole–Frenkel emission [79], [80]. Other studies, based on the measurement of the device local temperature [84] or thermal modeling, especially considering the effect of phase coexistence [70], [71], [85], [86], point out contribution from thermal effects in direct current (dc) E-MIT [85]–[88]. Furthermore, the temperature rise as a result of Joule heating may also result in nonlinear I–V curves. In a dc measurement, even if E-MIT were initially triggered electronically, the large ON-state current would induce large local temperature change. Therefore, one needs to go to high fields and short pulses to minimize the heating energy dissipated in order to study the E-MIT mechanisms, as will be discussed in Section IV-A.

Other types of switching behavior can also be observed in two-terminal devices. Nonvolatile switching has been observed in a family of Mott insulators AM_4X_8 (A= Ga, Ge; M = V, Nb, Ta; X = S, Se), which was attributed to electrically triggered MIT [89]–[91]. Further studies are needed to address the questions on what is the relative importance of the electron correlation versus direct structural change as in PCRAMs. Multistate nonvolatile resistance change has been achieved in VO_2 through Joule heating in the hysteresis window [72].

In a three-terminal transistor-type devices, there is yet another way to induce carrier density change, i.e., electrostatic carrier doping through field effect, which would not involve Joule heating because of low gate-drain current [92]. Attempts to trigger Mott transitions in solid-state field-effect transistors have been made with materials like VO_2 [81], [93], [94], cuprates [95], and other correlated oxides [92]. However, the areal carrier density induced with solid dielectrics is usually insufficient to drive the phase transitions in most cases [96], [97]. Recently, there has been growing interest in using liquid-based electrolyte gating in electric double-layer transistors (EDLTs) to create high-density surface charge and, therefore, phase transitions [98]–[101]. Many such devices show hysteretic gating behaviors [102]–[104] that are of relevance to nonvolatile memory. The origin of hysteresis in such devices, however, is related to the compositional changes occurring at the electrolyte–oxide interface and distinct from undercooling mechanisms [105], [106].

G. Materials Synthesis

A problem often encountered in the growth and fabrication process of Mott insulators is that the MIT transition ON/OFF ratio is often smaller in thin films than in single crystals or becomes degraded after fabrication. This originates from the fact that transition metals can usually have multiple valence states, and there could be multiple crystallographic phases for a single stoichiometry. The anisotropy of crystal phases also leads to differences in ease of ion migration and therefore different activation barriers for oxidation/reduction of the anion sublattice. The interplay between different degrees of freedom makes the electrical properties extremely sensitive to deviation from stable crystal structures, nonstoichiometry, and defects. The ability to modify crystal composition by interstitial doping or metastable incorporation of dopants can lead to emergence of new electronic phases. Consequently, the growth of these materials often requires careful control of temperature, stoichiometry, and defects to achieve large ON/OFF ratio. Significant progress has been made on both epitaxial [107]–[109] and nonepitaxial growths [110] of high-quality Mott insulators by PLD [111]–[113], sputtering, e-beam evaporation [114], atomic layer deposition [115], [116], chemical vapor deposition [117], [118], molecular beam epitaxy [119], [120], and sol-gel methods [121] in the form of thin films [122]–[125] and

nanostructures [126]–[130]. Low-temperature deposition techniques combined with postannealing procedures have also been widely studied [115], [131]. Recently, it was demonstrated that the resistivity of $SmNiO_3$ can change by eight orders of magnitude by electron doping, many orders of magnitude larger than its thermal MIT [132]. Such colossal resistance change is due to the band structure change of Mott insulators upon carrier doping. This can inspire the idea of using reversible ionic doping (controlled by electric field and independent of temperature) to achieve larger ON/OFF ratio than what is typically achievable in a thermal phase transition and forms the basis for a new research direction.

III. MOTT-INSULATOR-BASED MEMORY DEVICES

A. Mott Selectors in 1S1R Arrays

Mott insulators may be utilized as selector devices in the cross-point nonvolatile memory arrays such as for RRAM or PCRAM. Cross-point arrays shown in Fig. 7(a) offer one of the densest packing for nonvolatile RRAM and PCRAM with a cell size as small as $4F^2$. However, with a single RRAM or PCRAM as the memory unit, the current can sneak through undesired pathways, leading to read/write errors. As a result, a selector device with either nonlinear or asymmetric current–voltage characteristics (e.g., a diode or a transistor) needs to be integrated with each RAM cell to form a 1-selector–1-RRAM (1S1R) array [133]. Fig. 7(b) shows a 1S1R cross-point array with Mott-insulator-based threshold switches as the selectors. Because there are no junctions in Mott-insulator-based selectors, such structures could be more stackable, more compact, and easier to fabricate than typical diodes and transistors. What is more, Mott selectors may be especially useful for bipolar switching RRAMs as they allow large current to pass in both directions unlike diodes. As a result, there have been several studies investigating selector properties of VO_2 and NbO_2 [134]–[144].

The operational principle of a selector is as follows.

1) Reading of an HRS unit: During this step, when a read voltage V_{read} is applied to the selected HRS cell, the total current needs to be low. A large sneak current will appear if all of the other cells are ON. In such an extreme case, the maximum voltage drop on any unselected cell will be half of the read voltage in a large array. Now if a Mott selector is added to each of the memory cell and its threshold voltage $V_{\mathrm{th}} > 1/2V_{\mathrm{read}}$, all the unselected Mott selectors stay OFF. In this way, the sneak current will be limited by the OFF resistance of the Mott selectors. Note that the Mott selector of the chosen HRS can still be turned ON without setting the memory to LRS if I_{th} is lower than I_{set}, and it is usually the case. In addition, the Mott selector of the chosen HRS could, in principle,

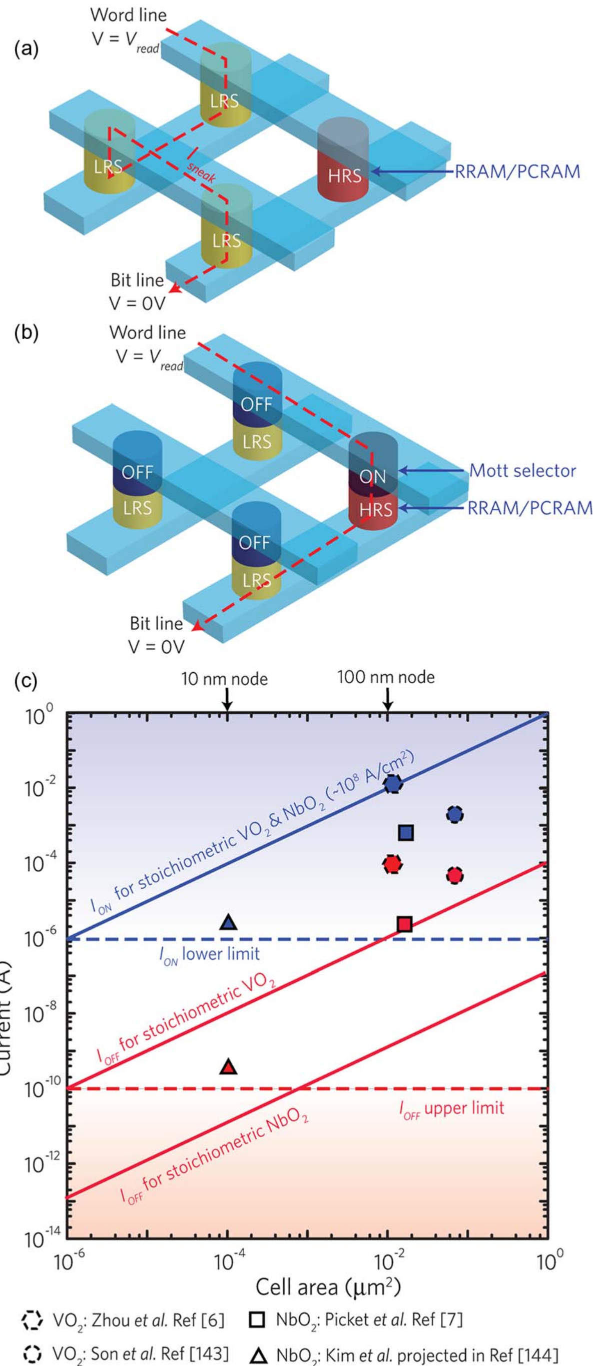

Fig. 7. *(a) Cross-point array enables high-density stackable packing of nonvolatile memories (RRAMs or PCRAMs), but suffer from sneak path current problems when each unit only contains a memory. (b) Using Mott two-terminal threshold switches as selectors can prevent sneak current problems. Note that the selected Mott switch does not necessarily have to be ON if the selected memory is in the HRS state. (c) The design space of Mott selector devices considering the criterion for the ON/OFF current. The weak scaling or nonscaling of ON resistance and current due to the filamentary conduction in RRAMs imposes strict restrictions on the material choice for Mott selector devices whose conductance scales with device area. Experimental data are taken from [6], [7], [143], and [144]. Blue filling corresponds to ON current while the red symbols represent OFF current.*

stay OFF, as the total current is distinguishable from the ON-state.

2) Reading of an LRS unit is trivial. When the selected RRAM is in its LRS state, the selector will not impede the current flow as long as $V_{th} < V_{read}$.
3) Setting/resetting (writing) the unit: in the writing process, the current through the memory and selector should be large enough not only to turn the selector ON, but also to SET/RESET the memory. This requires the selectors to have relatively large current density in the ON-state, because of the relative large SET/RESET current of the RRAM. There are ongoing efforts in reducing the SET/RESET current, which will not only put less restrictions on the selector and related circuit design, but also lowers the power consumption [145]. Another restriction is that the write voltage however should not be too large to change the state of nonselected memories in the sneak paths. A simple implement would require $V_{write} < 2V_{th}$, while less strict criterion could also be designed depending on the resistance ratio of the memory and selector elements.

Mott insulator selectors and RRAM have significantly different scaling behaviors (see Table 1) because of their different resistive switching mechanism. Since the threshold switching in Mott insulators is due to the bulk phase transition between the insulating and metallic phase, both the ON-state and OFF-state resistances will scale with device area as for a simple rectangular resistor with uniform resistivity. On the contrary, resistive switching in RRAM is facilitated by the formation and rupture of conductive filaments, leading to the weak scaling or even nonscaling of the SET/RESET current and ON-state resistance, etc. (see [145], [146], and reference therein). In principle, the CF conduction in RRAM would also confine the current flow cross section in the selector. In the following discussion, we assume no such confinement effect, which can be achieved by, e.g., inserting a metal electrode between the memory and the selector.

Of course, besides the threshold voltage, resistances of the RRAM and selector have to match with each other in the 1R1S memory arrays. The resistance of the HRS and the LRS of the memory unit is referred to as R_{HRS} and R_{LRS}, respectively, while the resistance of the ON-state and the OFF-state of the Mott selector is denoted as R_{ON} and R_{OFF}. Fig. 7(c) illustrates the design space of Mott selectors in RRAM 1S1R arrays. First, the ON-state current of a selector has to be high enough to SET/RESET the memory unit. The program (SET/RESET) current of RRAM is typically ~1–100 μA independent of the cell size [145], [147]–[153], which sets the 1-μA lower limit of the ON-state current of the Mott selector, as shown in Fig. 7(c). On the other hand, the OFF-state current of the selector must be low enough to prevent error readings due to the sneak current, especially when there are a large number of memory units in the 1S1R array. The total read current I_{read_H} is the current across the selected HRS unit plus the sneak current paths across all other memory units ($I_{read_H} = I_{HRS} + I_{sneak}$). The current across the selected HRS unit is given by $I_{HRS} = V_{read}/R_{HRS}$, because the selector is switched ON by V_{read}. In a 1S1R array with $n \times n$ units (n being 1024 typically), the sneak current can be calculated from $I_{sneak} = V_{read}/R'$, where R' is the effective resistance of the nonselected resistor network. The effective resistance of the remaining network will be the largest if all other memory units are in LRS except the selected one and can be estimated to be $R'(R_{LRS} + R_{OFF})/n$.

In order to be able to preserve the same ON/OFF ratio of the RRAM or PCRAM in a circuit as in single device, the sneak current has to be smaller than the HRS current, $I_{sneak} < I_{HRS}$. In other words, the sneak current across a single nonselected cell must be n times smaller than the read current of the selected HRS cell in an $n \times n$. If $R_{HRS} > 10^3 R_{LRS}$, this leads to $R_{OFF} > 10^6 R_{LRS}$. However, we could, in fact, impose a less strict requirement on the sneak current. As long as the total current HRS read current ($I_{read_H} = I_{HRS} + I_{sneak}$) is ten times smaller than the LRS read current, i.e., $I_{read_L} > 10 I_{read_H} \sim 10 I_{sneak}$, it would be sufficient to differentiate the resistance states of the memory. This means that the insulating resistance of the selector must satisfy $R_{OFF} > 10^4 R_{LRS}$. The above analysis sets the upper limit of the OFF-state current of about 0.1 nA, as illustrated in Fig. 7(c).

As a result, a selector cell must have an ON current over the horizontal dashed blue line and an OFF current below the dashed red line. For a Mott selector, the ON/OFF-state current is given by $I = jA = \sigma EA$, where A is the cell size, j is the current density, E is the applied electric field, and σ is the conductivity in the corresponding phase. The read electric field E should be comparable to the switching threshold E_T (typically 10^4–10^5 V/cm) and be constant as the driving voltage scales with the vertical dimension. The resistivity of single crystal VO_2 for example changes from 10 Ω·cm at room temperature to ~10^{-3} Ω·cm above the transition temperature in the metallic phase. Plugging in the values of resistivity of both phases and the electric field, we can plot both I_{ON} and I_{OFF} versus cell size curves for a VO_2 selector device, as shown in Fig. 7(c). Because

Table 1 Summary of Scaling Behavior of RRAM and Mott Selector

	RRAM [145]	Mott selector
Lateral dimension	λ	λ
Vertical dimension	λ	λ
High resistance	1/λ	1/λ
Low resistance	1	1/λ
V_{Th}	N/A	λ
RESET current	Weak scaling	N/A
ON current	N/A	$1/\lambda^2$

the resistivity of nonstoichiometric VO_2 is lower than that of stoichiometric VO_2 in the insulating phase and higher in the metallic phase, I_{ON} and I_{OFF} versus cell size curves practically set the upper limit of I_{ON} and the lower limit of I_{OFF} of a VO_2 selector. The region between these two lines is the achievable design space for VO_2 selectors. From Fig. 6(c), it is clear that I_{ON} of VO_2 is sufficiently large to drive the program current of the memory unit for node dimension down to 1 nm (current density $\sim 10^8$ A/cm^2). However, the OFF-state current would be larger than 0.1 nA with the node size larger than 1 nm, giving rise to a too large sneak current over the entire array. Only VO_2 selectors with node size $\sim$1 nm have high enough resistance in the insulating phase while simultaneously satisfying the criterion for I_{ON}. The feasibility of such a design is still elusive as studies on devices approaching sub-10 nm are still in early stages.

The ON/OFF ratio of the selector must be at least four orders of magnitude ($R_{OFF} > 10^4 R_{LRS} \sim 10^4 R_{ON}$). In practice, it is challenging to fabricate VO_2 devices with ON/OFF ratio approaching the ideal case in cross-point fashion, as the grown VO_2 films are typically nonstoichiometric on elemental metal electrodes. Experimental results of I_{ON} and I_{OFF} for VO_2 cells with cell area smaller than 1 μm^2 are shown as dots in Fig. 7(c). It can be clearly seen in these devices that the ON/OFF ratio is only around two orders of magnitude. How to grow high-quality VO_2 thin films on a specific substrate while maintaining the transition magnitude that is close to bulk has become a key problem and will motivate new ideas for materials synthesis beyond tweaking deposition parameters.

From the above discussion, we can see that only certain VO_2 devices with a specific cell area can fulfill the requirement for ON and OFF current. On the other hand, if there were another material with a larger transition magnitude, the requirement on the cell size would be much less strict. One of the potential candidate materials is NbO_2. Although the resistivity change of NbO_2 right across the metal-to-insulator transition temperature is only two to three orders of magnitude, its resistivity can be more than $\sim 10^4$ $\Omega\cdot$cm at room temperature and $\sim 10^{-3}$ $\Omega\cdot$cm above the transition temperature T_C ($\sim$1070 K) [154]. This is due to its larger insulating bandgap compared with VO_2 and much higher T_C. If the transition magnitude can be realized by a voltage bias, it would in theory offer a much larger design space, as shown in Fig. 7(c). Experimentally, NbO_x-based selector devices with high ON current density ($> 3 \times 10^7$ A/cm^2) and high selectivity ($\sim 10^4$) have been demonstrated [138], [139]. What is more, it was shown that the selector current path can be confined in a hybrid NbO_2/Nb_2O_5 or NbO_2/HfO_2 device and therefore reduce the effective device area [140]. As both ON and OFF switching speeds of a 110×110 nm^2 device are within $\sim$1–2 ns [7], the application of NbO_2 selectors would be of significant interest if near-ideal selectivity could be demonstrated. Another advantage of NbO_2-based selectors is that they could be more reliable than the VO_2 counterparts, as the transition temperature is much higher than the typical CMOS junction temperature. A master list of correlated electron phase transitions with respective ON/OFF ratios can be found elsewhere [155].

When the oxides are nonstoichiometric, or stoichiometric but not in a specific crystallographic phase, they would not exhibit metal-to-insulator transitions and could not be utilized as selectors. However, bipolar nonvolatile switching could be observed in these oxides (for example, amorphous VO_x deposited at room temperature [73], [74]). It is, therefore, possible to observe the coexistence of bipolar nonvolatile switching and threshold switching in inhomogeneous correlated materials [156], and such devices could even be self-selective, which may lead to simple one-element RRAM devices [157].

B. Capacitive Memories

Because the electronic phase transitions are often accompanied by the change in the dielectric properties [158]–[160] (from lattice and electronic change), Mott memories based on the change in capacitance have also been proposed. Fig. 8(a) shows the structure of a single

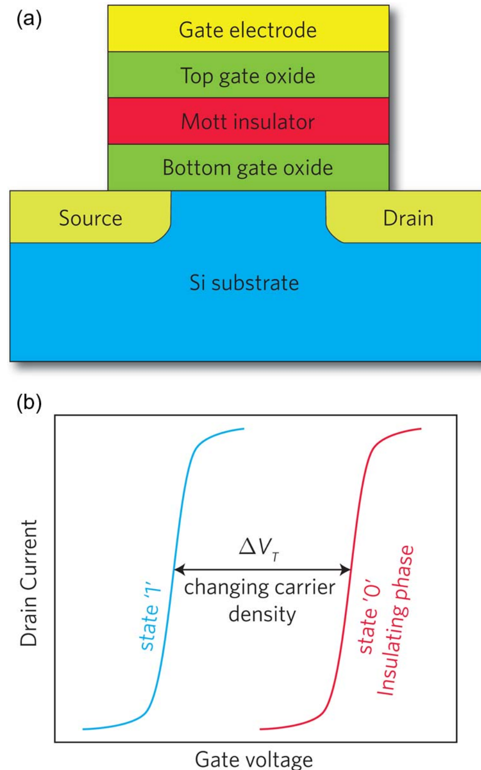

Fig. 8. *(a) The structure of a single element phase transition memory. (b) The changes in free carrier density in the Mott material modifies the effective gate capacitance and shifts the threshold voltage of the field-effect transistor by ΔV_T. (Panel (a) adapted with permission from [161].)*

element phase transition memory [161], [162], which is very similar to a Flash memory. A layer of Mott insulator is sandwiched between two gate oxide layers, which forms the gate oxide stack of a metal–oxide–semiconductor field-effect transistor (MOSFET). The effective gate capacitance would be different for insulating and metallic phases of the Mott insulator. In the ideal case, the effective gate capacitance is the series capacitance of three oxide layers when the sandwiched correlated oxide is in its insulating phase, and will only have contributions from the top and bottom gate oxide when the Mott insulator switches. This would lead to a drift in the threshold voltage of the MOSFET, as illustrated in Fig. 8(b). As a result, the state of the device can be read from the source–drain conductance under a specific gate voltage. Kim *et al.* showed that the MOSFET threshold voltage can be shifted by 0.5 V when using VO_2 as the phase transition element [161]. Recently, it has been found that the gate electric field induces space charge polarization from ionized defects in a SNO-based memory device [89], [163]. It is interesting to note that the retention time after a gate pulse is on the order of $\sim$10 s, longer than DRAM retention time, with a single transistor. Similarly, capacitance and inductance memory effects [164] enable the demonstration of memory metamaterials [165]–[168].

C. Neuromorphic Devices: Neuristors

In comparison with conventional digital computers, biological brains are massively parallel, faster, and more power efficient at certain tasks like image recognition and natural language processing [169]. There is growing interest in artificial neural circuits with the long-term goal of building computers mimicking the human brain and even helping to understand the brain function on a system level. The simulation of a brain at the software level is energy and space intensive [170]. As an example, a recent demonstration by Google of recognizing cats and human faces from video clips required 16 000 cores and $\sim$100 kW of power [171]. Therefore, there is a resurgent trend in investigating the hardware-level implementation of neuromorphic computation [172]–[175]. The active area and power consumption are two primary concerns for hardware design. The implementation of neuromorphic computing on the basis of conventional complementary metal–oxide–semiconductor (CMOS), however, often requires a large numbers of transistors to simulate single neuron or synapse. For example, 147 456 processors (10^9 B per processor) and 10^{14} B of memory were used to simulate 10^9 neurons and $\sim 10^{13}$ partially plastic synapses [172]. The power consumption was estimated at the level of hundreds of kilowatts [176]. The recent IBM TrueNorth chip used 5.4 billion transistors to mimic one million neurons and 256 million nonplastic synapses, with newly designed architecture [174]. To realize synaptic plasticity would require significantly more transistors. The inherent inefficiencies in simulating brains with CMOS are related to the digital versus analog way that CMOS circuits and the brain work, respectively. As a result, the question arises whether one can go below the architecture level and look for innovations at the materials or device level to use much fewer electronic devices to simulate the neurons and synapses. For example, RRAM may be used as a single device to mimic the synapse [175], [177]. The use of Mott insulators in neuromorphic devices is emerging in this context as an effective way to simulate neurons and synapses on a device level. In Sections III-C and III-D, we examine the motivation behind the use of correlated insulators in realizing electronic neurons and synapse, and discuss the related device performance and potential.

Neurons generate and transmit information through electrical and chemical signals. Each neuron possesses a body cell, which generates electrical spikes; an axon, which sends signals to other neurons; and dendrites, which receive signals. A synapse is a structure that permits the signal to transfer from the axon terminal of one cell and the dendrites of another, and its connection strength can be modulated, which is believed to lay the foundation of memories.

The electrical spiking signals in neurons, so called action potentials, are caused by the change in the ion concentrations (e.g., Na^+ and K^+) within and outside the neuron cell body. The generation and propagation of action potentials relies on the pumping of the ions by voltage-gated ion channel and has been described by a set of nonlinear differential equations, that is the well-known Hodgkin–Huxley model [178]. Recently, it has been suggested by Pickett *et al.* [179] that the behavior of neurons initiating action potentials can be emulated by a neuristor that is built from two Mott threshold switches along with resistors and capacitors. Fig. 9(a) shows the circuit diagram of a neuristor. Two identical Mott switches, M_1 and M_2, together with two parallel capacitances (C_1 and C_2), are biased by opposite dc bias to mimic the potassium and sodium ion channels in the Hodgkin–Huxley model. The input current charges the C_1 and C_2 capacitors before the voltage across M_1 and M_2 reaches their threshold voltage. When the threshold voltage is reached, the Mott insulator turns into metallic phase, leading to discharging of C_1 and C_2. The turning ON and OFF of the Mott switches is in analogy with the opening and closing of the ion channels, respectively. The offset between the charging/discharging time of the capacitors results in action potential voltage spikes, similar to biological systems. Fig. 9(b)–(e) shows the response of the circuit under two different stimulating input pulses. If the input voltage is superthreshold, the temporal profile of voltage output resembles that of biological action potentials and there is a maximum gain in the output voltage. On the other hand, when the input voltage is subthreshold, the output potential is weakened. Such response mimics the all-or-none law for neurons. The control of the interspike timing intervals and the spike width is achieved by modifying the capacitance value of C_1 and C_2. Fig. 9(f) shows various types of spiking behaviors achieved with different capacitance, indicating the versatility. It is worthwhile to

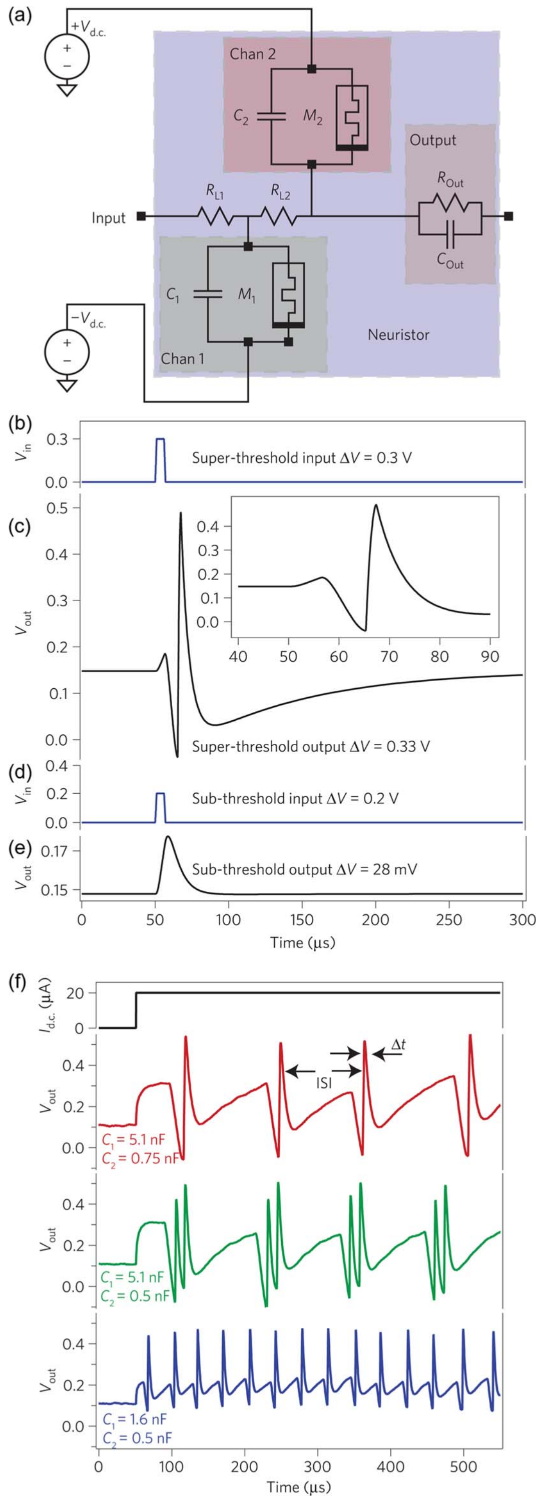

Fig. 9. *(a) Circuit diagram of a scalable neuristor made with Mott switches and normal capacitors. M_1 and M_2 are two identical threshold-switching devices made of NbO_2. (c) and (d) Superthreshold input and spiking-like output. (e) and (f) Subthreshold input and attenuated output. (g) Three types of spiking patterns: regular spiking, chattering, and fast spiking could be achieved in single circuit by adjusting the values of capacitors. (Adapted with permission from [179].)*

point out that neuristors have been demonstrated previously using other voltage-controlled negative differential resistance devices such as tunnel junctions [180], [181]. These designs usually require nonscalable inductors to operate [180], [181], while Mott switches can be scaled down to nanometer regime. Although the capacitors used were very large due to the large parasitic capacitance of the test apparatus, lowering the capacitance not only leads to reduced device area but also helps to generate higher frequency spikes and will be an important design criterion for more realistic circuits.

D. Neuromorphic Devices: Synaptic Transistor

As discussed above, neural cells can generate spikes under stimuli and the signal is passed on through synapses. Synaptic plasticity, the ability of synapses to strengthen or weaken, is believed to be the underlying mechanism of memory and learning. Spike-timing-dependent plasticity (STDP) is one where the synapse connection strength is adjusted based on the relative timing of a neuron's input (presynaptic) and output (postsynaptic) action potentials [182], [183]. Various types of STDP with different temporal dependency on spike timing have been observed. In the process of asymmetric STDP, the synaptic connection is strengthened if the presynaptic neuron fires before the postsynaptic neuron, and is weakened *vice versa*. The modification of strength is most significant if the input spikes occur immediately before/after the output spikes, as shown in Fig. 10(a). To emulate the synaptic function in electronic devices, the state (e.g., resistance) should be changed in a continuous fashion (analog) with reasonably long retention time (nonvolatile). Previously, artificial synapses have been implemented by two-terminal devices (for example, RRAM and PCRAM [175], [184]) and three-terminal FETs such as Si-based floating gate FET [185]. Recently, an ionic liquid-gated synaptic transistor has been demonstrated [186]. The transistor structure is shown in Fig. 10(b). The source and the drain are analogous to preneuron and postneuron terminals, respectively. The channel material is a perovskite $SmNiO_3$ (SNO), which exhibits a metal-to-insulator transition at $\sim$140 °C and its conductance S emulates the strength of synapse. The channel SNO is gated by a drop of ionic liquid, and the spike timing difference is translated into a gate bias signal pulse with varying magnitude lasting the same period of time. Ionic liquid gating has been used widely in the condensed matter physics community to tune the carrier density in Mott insulators electrostatically. However, recent studies have shown that there are electrochemical processes occurring in these transistors, especially under large gate bias, which create defects and therefore modify the transport properties of the material [105], [106]. The persistent and continuous change in conductivity as a result of electrochemical processes is beneficial for the realization of synaptic plasticity. When a positive gate voltage is applied, oxygen vacancies are created inside SNO, resulting in an increase in the channel

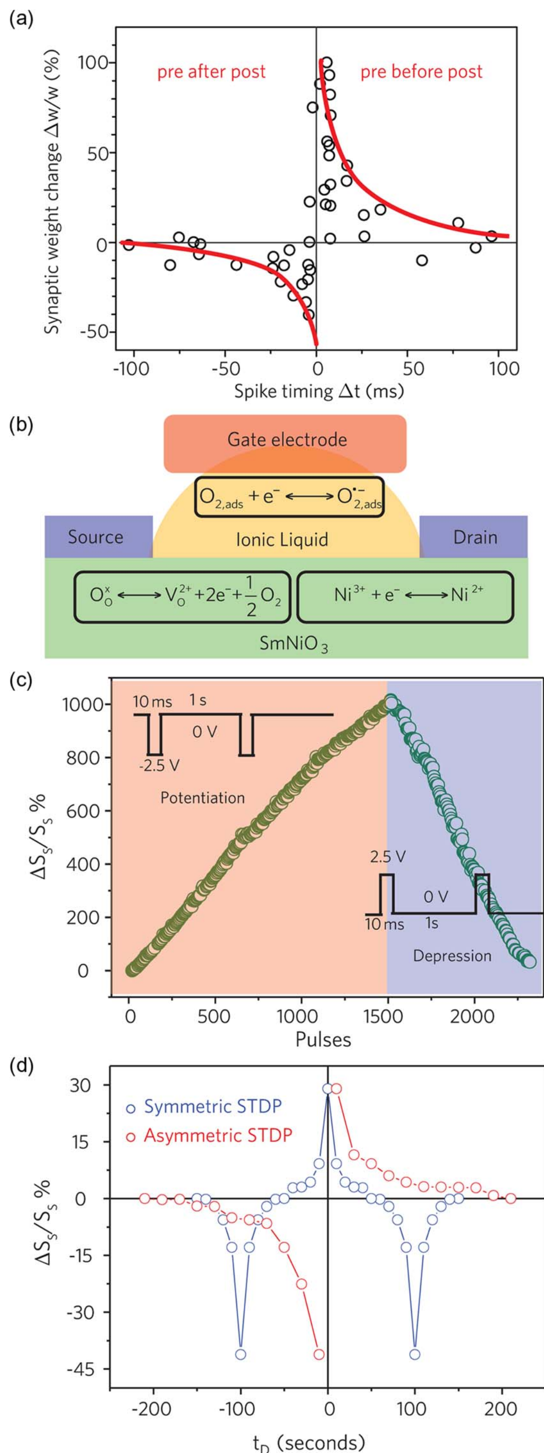

Fig. 10. *(a) Asymmetric spike-timing-dependent plasticity in a biological synapse. The synapse weight is adjusted as a function of the relative time of presynaptic and postsynaptic spikings. (b) Device structure of a synaptic transistor based on $SmNiO_3$, and the conductance modulation mechanism. (c) Sheet conductance S_S modulation of $SmNiO_3$ under potentiation and depression gate pulses. (d) Asymmetric and symmetric spike-timing-dependent plasticity demonstrated with a synaptic transistor. (Panel (a) adapted with permission from [183]; panels (b)–(d) adapted with permission from [186].)*

resistance. The overall defect reaction defect reaction in SNO can be written as $2Ni^{3+} + O_O^x \leftrightarrow 2Ni^{2+} + V_O^{2+} + 1/2O_2$. As discussed before, the electrical properties of Mott insulators in general are extremely sensitive to the carrier density and disorder, making them particularly suited. Fig. 10(c) shows the sheet conductance S_S modulation of SNO under potentiation and depression gate pulses (periodic 10-ms gate pulses repeated once per second). The conductance can be programed accumulatively in an analog fashion similar to synapse. Both asymmetric and symmetric STDPs can be demonstrated using such synaptic transistors along with a neuron circuitry to convert spike time difference to gate voltage, as shown in Fig. 10(d). Recently, device-level classical conditioning and unlearning have been realized using SNO synaptic transistors [187].

Several aspects of performance of such synaptic transistors remain to be improved. First, the conductance modulation is relatively small. Future devices utilizing ions with higher mobility could enable more significant conductance change in synaptic transistors. Second, the demonstrated three-terminal synaptic transistors are slower compared with two-terminal RRAM- and PCRAM-based synapses, but the speed would scale down with the device dimension. Confining ionic liquids by microfluidic techniques should greatly help in studying the limits of switching such liquid–oxide interfaces. What is more, the power/energy consumption of the electrochemical processes in these devices remains to be scrutinized. However, two-terminal synapses commonly operate with separated signal transmission and learning process, while these two processes occur simultaneously in biological synapses. Therefore, three-terminal synaptic transistors that are able to perform both operations concurrently may offer a promising path to efficient synapse emulation. In addition, the electrochemical transistor creates a defect diffusion profile at the channel surface, which could be better controlled than the stochastic defect creation in RRAM, and could therefore be more robust to device-to-device and cycle-to-cycle variations.

IV. KEY DEVICE PERFORMANCE METRICS

A. Limits of Switching Speed

One of the most prominent features of Mott insulators is that the transition can be induced at fast timescales. As can be seen from Table 2, many electronic transitions reflected by the change in electric and optical conductivity can take place within 10^2–10^3 fs when being triggered by optical excitations, comparable to transistor gate and interconnect delays. The experimental switching speed of voltage pulse-induced transitions is usually slower, on the order of a few nanoseconds, but still on par with RRAMs [145] and PCRAMs [188].

The optically induced transition dynamics of correlated insulators such as manganites [189], V_2O_3 [190], VO_2 [4],

Table 2 Metal-to-Insulator Transition Speed in Various Mott Insulators

Material	Driving method	Probe	Speed	reference
$Pr_{0.7}Ca_{0.3}MnO_3$	Mid-IR vibrational excitation	Reflectivity	1ps	[189]
$Pr_{0.7}Ca_{0.3}MnO_3$	Mid-IR vibrational excitation	Electrical conductivity	4 ns	[189]
V_2O_3	Voltage pulse	Electrical conductivity	390 ps	[203]
V_2O_3	Near-IR excitation	Far-IR conductivity	20 ps	[190]
VO_2	Voltage pulse	Electric conductivity	2 ns	[6]
VO_2	Near-IR excitation	Reflectivity	75 fs	[5]
VO_2	Near-IR excitation	Electron diffraction	300 fs	[40]
NbO_2	Voltage pulse	Electric conductivity	700 ps	[7]
1*T*-TaS_2	Near-IR excitation	Time-resolved ARPES	100 fs	[201]

[191]–[201], have been mostly studied by pump-probe techniques. In such experiments, a pump signal (typically with photon energy ~1.5 eV in the near-IR region, larger than the bandgap) creates enough number of electrons and holes in the conduction and valence band to collapse the gap, leading to nonthermal Mott transitions. A time-delayed probe is utilized to study various aspects of the transition dynamics. For example, an optical probe can detect the optical conductivity change, whereas ultrafast electron diffraction reveals structural transitions.

The interplay between different degrees of freedom is evident in ultrafast photoexcitation studies, which could potentially influence the speed of electronic phase transitions. Cavalleri *et al.* observed a transition speed bottle neck of $\sim10^2$ fs in the reflectivity/transmission change of VO_2 thin films after being optically excited, as shown in Fig. 11(a) [5]. The speed limit is attributed to the structural motion needed to collapse the bandgap. Baum *et al.* detected that the transition from stable insulating to metallic states will actually pass through a metastable phase [40]. The transition to the intermediate phase, characterized by local atomic motion and the dilation of the vanadium–vanadium bond, happens within ~300 fs and leads to the change in electrical conductivity. The slower relaxation from the intermediate to final tetragonal phase, manifested by the long-range atomic reordering and shear motion at sound wave velocity, takes a few picoseconds. This suggests that the electronic transition can occur simultaneously with local atomic motions, before the full crystallographic transition occurs.

The speed of voltage-triggered Mott transitions has been studied in both out-of-plane and in-plane two-terminal devices [6], [7], [64], [67], [202]–[206]. It is apparent that many factors such as material properties, device dimension, ambient temperature, and external electric field will influence the transition speed. Regardless, the reported values of switching ON time in VO_2, NbO_2, and other oxides range from $\sim10^{-1}$ to 10^1 ns [6], [7], [64], [67], [202]–[206]. Such speed is fast enough for many memory applications, considering that many of the reported values are still limited by parasitic capacitance and measurement instrumentation limitations [6], [205], [206]. Fig. 11(b) shows the current across a 400-nm-long VO_2 two-terminal device as the voltage ramps up [6]. Within 2 ns, the device resistance drops by two orders of magnitude, with similar magnitude as the thermal metal-to-insulator transition of the film.

The OFF time is an equally important parameter. Naturally, the device would become gradually easier to turn ON, but progressively more difficult to turn OFF with increasing ambient temperature, because of the decreasing free energy difference between the two phases. This leads to shorter switch ON but longer switch OFF times, as can be predicted by a simple thermal model. Accordingly, there would be an optimized operation temperature range in terms of the device's overall speed, as illustrated in Fig. 11(c) [207]. It is desirable to select a region where the ON/OFF times are not significantly modified by chip temperature fluctuations as a result of device operation. The choice of operation temperature will also have an influence on the device reliability. With high transition temperature, it may require extra thermal isolation/dissipation structures to prevent intervention with nearby circuit elements. A too low transition temperature on the other hand may cause unwanted switching as a result of chip temperature fluctuation.

B. Switching Energy of Phase Transitions

One of the most important considerations for any practical memory device is their energy cost [208]. The minimum energy consumption per switching is given by the free energy difference between two phases at the operation temperature.

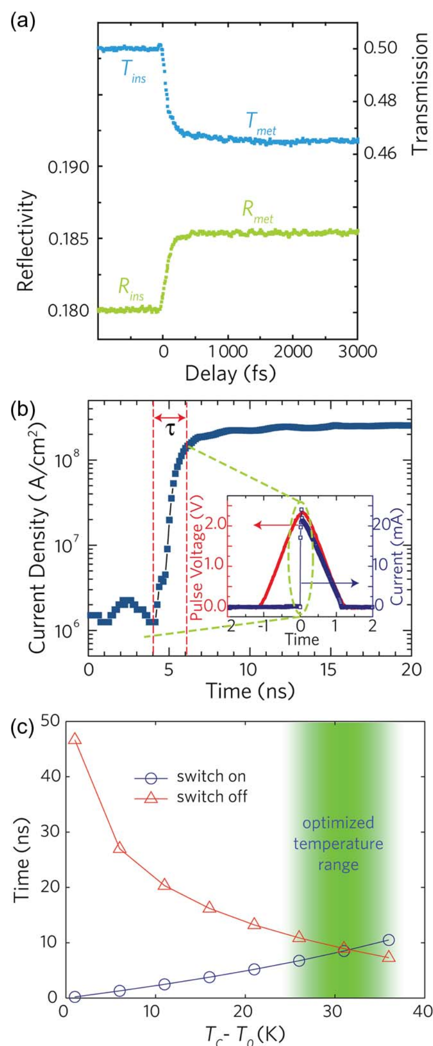

Fig. 11. *(a) Ultrafast phase transition in VO_2 as evidenced by reflection/transmission in optical pump-probe measurements. (b) Resistance change dynamics of a voltage-driven phase transition in VO_2. The inset shows both the voltage and current temporal profiles. (c) ON/OFF time as a function of operation temperature of a two-terminal Mott switch calculated by thermal modeling. (Panel (a) adapted with permission from [5]; panel (b) adapted with permission from [6]; panel (c) adapted with permission from [207].)*

Table 3 lists the volumetric average heat capacity and latent heat for different materials [7], [209]–[211]. One obvious advantage of Mott memories is that the switching energy per bit will scale with the volume of the device and could be therefore drastically decreased to sub-10-nm size. For example, the switching energy of a VO_2 or NbO_2 cube with length of 10 nm is estimated to be around a few fJ (∼0.4 fJ for VO_2 and ∼2 fJ for NbO_2), as estimated from the parameters in Table 3. It could also be seen that the energy cost to switch stoichiometric NbO_2 is larger than that of the same volume of stoichiometric VO_2. However, the heat capacity, phase transition latent heat, and transition temperature will also depend on material stoichiometry and defects. Thus, engineering techniques to reduce the energy per volume could be important to realize energy-efficient devices with large ON/OFF ratio.

C. Reliability

Reliability is one of the key concerns for Mott two-terminal switches especially if Joule heating plays an important role. Variations in the ON/OFF resistivity value are rather small, as shown in Fig. 12(a). The resistance of a single device can be changed by choosing the proper length and area. On the other hand, the initial E-MIT switching process could be stochastic as reflected in the variations in the V_{th} in Fig. 12(b). The initial partial switching could happen in different regions of the device as evidenced in optical microscopy studies. Reducing the device size to material grain size could be helpful to reduce such variations. On the other hand, there are usually less variations in the V^*_{th}, as the turnoff process is determined by the power input and heat dissipation in the device.

The variations between devices are related to the nonuniformity of the prepared thin films. Growth and processing techniques need to be optimized to achieve uniformity in the transition properties. In some cases, an electroforming process needs to be performed before the device could be switched on [59], which is possibly due to interfacial oxide layer formed at the metal/insulator interface and does not occur in all devices. From reliability point of view, devices without the need of electroforming are more desired, which requires proper selection of contact electrode materials. As for endurance, Radu *et al.* demonstrated that VO_2 switches have endurance better than 10^9 cycles [135]. Similar endurance performance has been demonstrated in NbO_2 [7]. Thin films confined to the substrate are more robust to the stress relaxation phenomena and this is in sharp contrast with bulk single crystals where the crystals shatter after one to few thermal cycles as a result of the structural transition.

D. (Non)Volatility of State

Devices based on correlated oxides can be either volatile or nonvolatile depending on their operation principles. The switching is volatile for voltage triggered MIT in NbO_2 and VO_2, because the transitions are either induced by injecting extra carriers or Joule heating (also referred to as threshold switches). For both cases, the metallic phase cannot be sustained once external driving force is removed. On the other hand, if the MIT is driven by carriers that are created (or annihilated) from defect density changes as in the synaptic transistor discussed above, the device will operate in a nonvolatile fashion, since the defects persist once created. Both volatile and nonvolatile behaviors have been demonstrated, and one can choose the desired operation principle/properties based on the applications. For neuromorphic circuits, the synapses need to be nonvolatile whereas the neurons are composed of volatile elements. In nickelate synaptic transistors for instance, due to low

Table 3 Volumetric Free Energy Cost for Phase Transitions

Material	Volumetric heat capacity a, b	Volumetric enthalpy of transformation b	Transition temperature b	Total volumetric enthalpy b	Reference
NbO_2	2.6×10^6 J m^{-3} K^{-1}	1.6×10^8 J m^{-3}	1070 K	2.2×10^9 J m^{-3}	[7,209]
VO_2	3.0×10^6 J m^{-3} K^{-1}	2.4×10^8 J m^{-3}	340 K	3.6×10^8 J m^{-3}	[210, 211]

[a] Heat capacity value is temperature dependent and taken as the average from room temperature to the transition temperature.
[b] The given numbers serve as references and only apply to stoichiometric transition metal oxides with specific crystal structure. The exact values of these physical constants depend on the sample's stoichiometry and can be tuned over a wide range.

diffusivity of defects in solids at room temperature, the channel resistance does not degrade even after a few months. The retention properties of these devices would certainly be interesting for future studies.

V. OUTLOOK AND FUTURE RESEARCH NEEDS

Orbitronic memory devices that utilize collective state switching are being actively explored in the materials sciences and device community. Many device parameters, including switching voltage and speed, are compatible with RRAMs and PCRAMs to form 1S1R nonvolatile memory arrays, while the ON/OFF ratio still needs to be improved. Thermal stability of phase change switches in highly integrated circuits requires attention. Radiation effects on correlated insulators and device reliability is another area that calls for much emphasis. Device physics models that can capture correlation effects even to an approximate level therefore are essential. While first principle studies can provide critical insights into many aspects of the materials, often they cannot capture the whole spectrum of complex phenomena in real materials. Mott materials are of interest in capacitive memories in Flash-like structures. The application of Mott insulators in neuromorphic devices is in early stages, and it may be possible to monolithically integrate such neural elements with conventional Si devices to form brain-inspired circuits. The ability to continuously tune the electrical resistance of Mott insulators, time-dependent resistance modulation as well as obtain high nonlinearity positions them uniquely in such circuits.

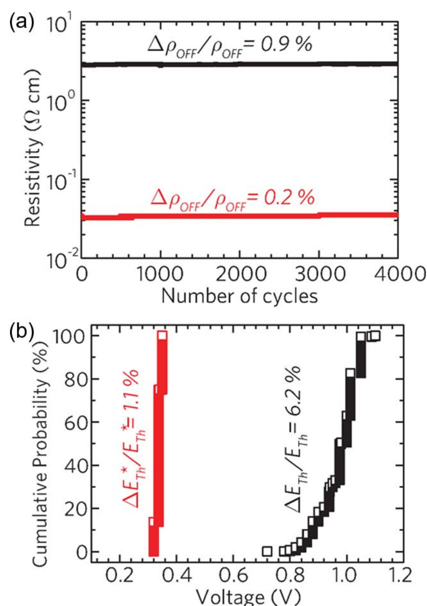

Fig. 12. *Variation of (a) ON/OFF resistance and (b) threshold voltage of a VO_2 two-terminal device over a few thousand cycles.*

At the same time, many important questions remain. The underlying physical mechanisms of MIT under various excitation sources need to be studied. Whether the final electronic states are identical regardless of the excitation source requires combined *in situ* probes. Many of the existing studies have been performed on vanadium dioxide partly due to the proximity of the transition to room temperature and ease of applying various experimental techniques. For materials showing transitions at higher temperature such as nickelates and niobium oxides, there is still plenty to be understood. New instrumentation will be needed to perform even the most basic *in situ* experiments due to the environmental (oxygen partial pressure) control needed to maintain the phase and compositional stability. Modeling the scaling behavior of memory devices requires deeper understanding of the electronic band structures of Mott insulators. High-quality heterojunctions or homo p-n junctions are certainly helpful to understand basic electrostatics. The electrical properties of interfaces between Mott insulators and band insulators (i.e., gate dielectric)/metals (i.e., contacts) become increasingly important as devices scale down, which we know very little of. In turn, this implies that we need to be able to control defects at the oxide interfaces to a minimum to probe the intrinsic properties. Dispersive capacitance in such complex oxides often poses a challenge in applying commonly used

capacitance–voltage curve analysis to understand electrical nature of gate stack interfaces.

From a materials perspective, the growth of Mott insulators has been challenging because of defects and nonstoichiometry related degradation of the transition magnitude (i.e., ON/OFF ratio). While epitaxial growth of oxides on lattice-matched single crystal substrates is mature, growth of phase-pure films on nonlattice matched substrates such as metals and atomic layer deposited oxides in a CMOS-compatible process is an area that requires intense effort. On the other hand, controlled defect creation by electric fields modifies orbital occupancy of correlated electrons and induces nonvolatile resistance changes. Exploiting the great sensitivity of their electrical properties to defects could, therefore, lead to novel applications in ionic–electronic devices. Collaborative efforts between material growers and device engineers will advance the frontiers of this field in the coming decades and will foster the growth of orbitronics. ■

REFERENCES

[1] J. H. de Boer and E. J. W. Verwey, "Semi-conductors with partially and with completely filled 3D-lattice bands," *Proc. Phys. Soc.*, vol. 49, p. 59, 1937.

[2] N. F. Mott, "The basis of the electron theory of metals, with special reference to the transition metals," *Proc. Phys. Soc. A*, vol. 62, p. 416, 1949.

[3] N. Mott, "On metal-insulator transitions," *J. Solid State Chem.*, vol. 88, pp. 5–7, 1990.

[4] A. Cavalleri *et al.*, "Femtosecond structural dynamics in VO_2 during an ultrafast solid-solid phase transition," *Phys. Rev. Lett.*, vol. 87, 2001, Art. ID. 237401.

[5] A. Cavalleri, T. Dekorsy, H. H. W. Chong, J. C. Kieffer, and R. W. Schoenlein, "Evidence for a structurally-driven insulator-to-metal transition in VO_2: A view from the ultrafast timescale," *Phys. Rev. B*, vol. 70, 2004, Art. ID. 161102.

[6] Y. Zhou *et al.*, "Voltage-triggered ultrafast phase transition in vanadium dioxide switches," *IEEE Electron Device Lett.*, vol. 34, no. 2, pp. 220–222, Feb. 2013.

[7] M. D. Pickett and R. S. Williams, "Sub-100 fJ and sub-nanosecond thermally driven threshold switching in niobium oxide crosspoint nanodevices," *Nanotechnology*, vol. 23, 2012, Art. ID. 215202.

[8] International Technology Roadmap for Semiconductors, 2013. [Online]. Available: http://www.itrs.net/Links/2013ITRS/Summary2013.htm

[9] Z. Yang, C. Ko, and S. Ramanathan, "Oxide electronics utilizing ultrafast metal-insulator transitions," *Annu. Rev. Mater. Res.*, vol. 41, pp. 337–367, 2011.

[10] M. M. Qazilbash *et al.*, "Mott transition in VO_2 revealed by infrared spectroscopy and nano-imaging," *Science*, vol. 318, pp. 1750–1753, 2007.

[11] J. Wei, Z. Wang, W. Chen, and D. H. Cobden, "New aspects of the metal-insulator transition in single-domain vanadium dioxide nanobeams," *Nature Nanotechnol.*, vol. 4, pp. 420–424, 2009.

[12] J. Cao *et al.*, "Strain engineering and one-dimensional organization of metal-insulator domains in single-crystal vanadium dioxide beams," *Nature Nanotechnol.*, vol. 4, pp. 732–737, 2009.

[13] I. I. Mazin *et al.*, "Charge ordering as alternative to Jahn-Teller distortion," *Phys. Rev. Lett.*, vol. 98, 2007, Art. ID. 176406.

[14] E. Verwey, "Electronic conduction of magnetite (Fe_3O_4) and its transition point at low temperatures," *Nature*, vol. 144, pp. 327–328, 1939.

[15] J. A. Alonso *et al.*, "High-temperature structural evolution of $RNiO_3$ (R = Ho, Y, Er, Lu) perovskites: Charge disproportionation and electronic localization," *Phys. Rev. B*, vol. 64, 2001, Art. ID. 094102.

[16] M. Imada, A. Fujimori, and Y. Tokura, "Metal-insulator transitions," *Rev. Modern Phys.*, vol. 70, pp. 1039–1263, 1998.

[17] J. M. Rondinelli, S. J. May, and J. W. Freeland, "Control of octahedral connectivity in perovskite oxide heterostructures: An emerging route to multifunctional materials discovery," *MRS Bull.*, vol. 37, pp. 261–270, 2012.

[18] J. B. Goodenough, "Electronic and ionic transport properties and other physical aspects of perovskites," *Rep. Progr. Phys.*, vol. 67, p. 1915, 2004.

[19] N. F. Mott and L. Friedman, "Metal-insulator transitions in VO_2, Ti2O3 and $Ti_{2-x}V_xO_3$," *Philosoph. Mag.*, vol. 30, pp. 389–402, 1974.

[20] A. P. Ramirez, "Colossal magnetoresistance," *J. Phys., Condensed Matter*, vol. 9, pp. 8171–8199, 1997.

[21] S. M. Wu *et al.*, "Reversible electric control of exchange bias in a multiferroic field-effect device," *Nature Mater.*, vol. 9, pp. 756–761, 2010.

[22] S. Fusil, V. Garcia, A. Barthélémy, and M. Bibes, "Magnetoelectric devices for spintronics," *Annu. Rev. Mater. Res.*, vol. 44, pp. 91–116, 2014.

[23] A. I. Khan *et al.*, "Negative capacitance in a ferroelectric capacitor," *Nature Mater.*, vol. 14, pp. 182–186, 2015.

[24] J. B. Goodenough, "The two components of the crystallographic transition in VO_2," *J. Solid State Chem.*, vol. 3, pp. 490–500, 1971.

[25] A. Zylbersztejn and N. F. Mott, "Metal-insulator transition in vanadium dioxide," *Phys. Rev. B*, vol. 11, pp. 4383–4395, 1975.

[26] R. M. Wentzcovitch, W. W. Schulz, and P. B. Allen, "VO_2: Peierls or Mott-Hubbard? A view from band theory," *Phys. Rev. Lett.*, vol. 72, pp. 3389–3392, 1994.

[27] V. Eyert, "VO_2: A novel view from band theory," *Phys. Rev. Lett.*, vol. 107, 2011, Art. ID. 016401.

[28] T. M. Rice, H. Launois, and J. P. Pouget, "Comment on VO_2: Peierls or Mott-Hubbard? A view from Band theory," *Phys. Rev. Lett.*, vol. 73, pp. 3042–3042, 1994.

[29] R. Eguchi *et al.*, "Photoemission evidence for a Mott-Hubbard metal-insulator transition in VO_2," *Phys. Rev. B*, vol. 78, 2008, Art. ID. 075115.

[30] M. W. Haverkort *et al.*, "Orbital-assisted metal-insulator transition in VO_2," *Phys. Rev. Lett.*, vol. 95, 2005, Art. ID. 196404.

[31] J. P. Pouget *et al.*, "Dimerization of a linear Heisenberg chain in the insulating phases of $V_{1-x}Cr_xO_2$," *Phys. Rev. B*, vol. 10, pp. 1801–1815, 1974.

[32] J. P. Pouget, H. Launois, J. P. D'Haenens, P. Merenda, and T. M. Rice, "Electron localization induced by uniaxial stress in pure VO_2," *Phys. Rev. Lett.*, vol. 35, pp. 873–875, 1975.

[33] S. Biermann, A. Poteryaev, A. I. Lichtenstein, and A. Georges, "Dynamical singlets and correlation-assisted peierls transition in VO_2," *Phys. Rev. Lett.*, vol. 94, 2005, Art. ID. 026404.

[34] A. Liebsch, H. Ishida, and G. Bihlmayer, "Coulomb correlations and orbital polarization in the metal-insulator transition of VO_2," *Phys. Rev. B*, vol. 71, 2005, Art. ID. 085109.

[35] J. M. Tomczak, F. Aryasetiawan, and S. Biermann, "Effective bandstructure in the insulating phase versus strong dynamical correlations in metallic VO_2," *Phys. Rev. B*, vol. 78, 2008, Art. ID. 115103.

[36] T. C. Koethe *et al.*, "Transfer of spectral weight and symmetry across the metal-insulator transition in VO_2," *Phys. Rev. Lett.*, vol. 97, 2006, Art. ID. 116402.

[37] A. S. Belozerov, M. A. Korotin, V. I. Anisimov, and A. I. Poteryaev, "Monoclinic M1 phase of VO_2: Mott-Hubbard versus band insulator," *Phys. Rev. B*, vol. 85, 2012, Art. ID. 045109.

[38] S. Kim, K. Kim, C.-J. Kang, and B. I. Min, "Correlation-assisted phonon softening and the orbital-selective Peierls transition in VO_2," *Phys. Rev. B*, vol. 87, 2013, Art. ID. 195106.

[39] J. D. Budai *et al.*, "Metallization of vanadium dioxide driven by large phonon entropy," *Nature*, vol. 515, pp. 535–539, 2014.

[40] P. Baum, D.-S. Yang, and A. H. Zewail, "4D visualization of transitional structures in phase transformations by electron diffraction," *Science*, vol. 318, pp. 788–792, 2007.

[41] H.-T. Kim *et al.*, "Monoclinic and correlated metal phase inVO_2 as evidence of the Mott transition: Coherent phonon analysis," *Phys. Rev. Lett.*, vol. 97, 2006, Art. ID. 266401.

[42] E. Arcangeletti *et al.*, "Evidence of a pressure-induced metallization process in monoclinic VO_2," *Phys. Rev. Lett.*, vol. 98, 2007, Art. ID. 196406.

[43] B.-J. Kim *et al.*, "Micrometer x-ray diffraction study of VO_2 films: Separation between metal-insulator transition and structural phase transition," *Phys. Rev. B*, vol. 77, 2008, Art. ID. 235401.

[44] K. L. Holman *et al.*, "Insulator to correlated metal transition in $V_{1-x}Mo_xO_2$," *Phys. Rev. B*, vol. 79, 2009, Art. ID. 245114.

[45] Z. Tao *et al.*, "Decoupling of structural and electronic phase transitions in VO_2," *Phys. Rev. Lett.*, vol. 109, 2012, Art. ID. 166406.

[46] J. Laverock *et al.*, "Direct observation of decoupled structural and electronic transitions and an ambient pressure monocliniclike metallic phase of VO_2," *Phys. Rev. Lett.*, vol. 113, 2014, Art. ID. 216402.

[47] W.-P. Hsieh *et al.*, "Evidence for photo-induced monoclinic metallic VO_2 under high pressure," *Appl. Phys. Lett.*, vol. 104, 2014, Art. ID. 021917.

[48] J. B. Hatch *et al.*, "Intermediate metallic phase in VO_2 observed with scanning tunneling spectroscopy," *Phys. Chem. Chem. Phys.*, vol. 16, pp. 14183–14188, 2014.

[49] D. Wegkamp *et al.*, "Instantaneous band gap collapse in photoexcited monoclinic VO_2 due to photocarrier doping," *Phys. Rev. Lett.*, vol. 113, 2014, Art. ID. 216401.

[50] S. Shin *et al.*, "Vacuum-ultraviolet reflectance and photoemission study of the metal-insulator phase transitions in VO_2,V_6O_{13}, and V_2O_3," *Phys. Rev. B*, vol. 41, pp. 4993–5009, 1990.

[51] S. A. Corr, D. P. Shoemaker, B. C. Melot, and R. Seshadri, "Real-space investigation of structural changes at the metal-insulator transition in VO_2," *Phys. Rev. Lett.*, vol. 105, 2010, Art. ID. 056404.

[52] H. H. Kung, *Transition Metal Oxides: Surface Chemistry and Catalysis*. Amsterdam, The Netherlands: Elsevier, 1989.

[53] N. F. Quackenbush *et al.*, "Nature of the metal insulator transition in ultrathin epitaxial vanadium dioxide," *Nano Lett.*, vol. 13, pp. 4857–4861, 2013.

[54] J. I. Sohn *et al.*, "Surface-stress-induced mott transition and nature of associated spatial phase transition in single crystalline VO_2 nanowires," *Nano Lett.*, vol. 9, pp. 3392–3397, 2009.

[55] R. G. Moore *et al.*, "A surface-tailored, purely electronic, Mott metal-to-insulator transition," *Science*, vol. 318, pp. 615–619, 2007.

[56] O. Friedt, "Structural and magnetic aspects of the metal-insulator transition in $Ca_{2-x}Sr_xRuO_4$," *Phys. Rev. B*, vol. 63, 2001, Art. ID. 174432.

[57] S. Nakatsuji *et al.*, "Heavy-mass Fermi liquid near a ferromagnetic instability in layered ruthenates," *Phys. Rev. Lett.*, vol. 90, 2003, Art. ID. 137202.

[58] S. Nakatsuji and Y. Maeno, "Quasi-two-dimensional Mott transition system $Ca_{2-x}Sr_xRuO_4$," *Phys. Rev. Lett.*, vol. 84, pp. 2666–2669, 2000.

[59] F. A. Chudnovskii, L. L. Odynets, A. L. Pergament, and G. B. Stefanovich, "Electroforming and switching in oxides of transition metals: The role of metal-insulator transition in the switching mechanism," *J. Solid State Chem.*, vol. 122, pp. 95–99, 1996.

[60] F. Chudnovskii, A. Pergament, G. Stefanovich, P. Metcalf, and J. Honig, "Switching phenomena in chromium-doped vanadium sesquioxide," *J. Appl. Phys.*, vol. 84, pp. 2643–2646, 1998.

[61] A. Asamitsu, Y. Tomioka, H. Kuwahara, and Y. Tokura, "Current switching of resistive states in magnetoresistive manganites," *Nature*, vol. 388, pp. 50–52, 1997.

[62] S. Lee *et al.*, "Electrically driven phase transition in magnetite nanostructures," *Nature Mater.*, vol. 7, pp. 130–133, 2007.

[63] S. Yamanouchi, Y. Taguchi, and Y. Tokura, "Dielectric breakdown of the insulating *charge-ordered state in* $La_{2-x}Sr_xNiO_4$," *Phys. Rev. Lett.*, vol. 83, pp. 5555–5558, 1999.

[64] J. Leroy *et al.*, "High-speed metal-insulator transition in vanadium dioxide films induced by an electrical pulsed voltage over nano-gap electrodes," *Appl. Phys. Lett.*, vol. 100, 2012, Art. ID. 213507.

[65] K. L. Chopra, "Current-controlled negative resistance in thin niobium oxide films," *Proc. IEEE*, vol. 51, no. 6, pp. 941–942, Jun. 1963.

[66] D. V. Geppert, "A new negative-resistance device," *Proc. IEEE*, vol. 51, no. 1, pp. 223–223, Jan. 1963.

[67] S. D. Ha, Y. Zhou, C. J. Fisher, S. Ramanathan, and J. P. Treadway, "Electrical switching dynamics and broadband microwave characteristics of VO_2 radio frequency devices," *J. Appl. Phys.*, vol. 113, 2013, Art. ID. 184501.

[68] R. Waser and M. Aono, "Nanoionics-based resistive switching memories," *Nature Mater.*, vol. 6, pp. 833–840, 2007.

[69] C. N. Berglund, "Thermal filaments in vanadium dioxide," *IEEE Trans. Electron Devices*, vol. 16, no. 5, pp. 432–437, May 1969.

[70] J. Sakai and M. Kurisu, "Effect of pressure on the electric-field-induced resistance switching of VO_2 planar-type junctions," *Phys. Rev. B*, vol. 78, 2008, Art. ID. 033106.

[71] J. Duchene, M. Terraillon, P. Pailly, and G. Adam, "Filamentary conduction in VO_2 coplanar thin-film devices," *Appl. Phys. Lett.*, vol. 19, pp. 115–117, 1971.

[72] L. Pellegrino *et al.*, "Multistate memory devices based on free-standing VO_2/TiO_2 microstructures driven by Joule self-heating," *Adv. Mater.*, vol. 24, pp. 2929–2934, 2012.

[73] M. Son *et al.*, "Self-selective characteristics of nanoscaleVO_x devices for high-density ReRAM applications," *IEEE Electron Device Lett.*, vol. 33, no. 5, pp. 718–720, May 2012.

[74] F. J. Wong, T. S. Sriram, B. R. Smith, and S. Ramanathan, "Bipolar resistive switching in room temperature grown disordered vanadium oxide thin-film devices," *Solid-State Electron.*, vol. 87, pp. 21–26, 2013.

[75] A. V. Pohm, C. Sie, R. Uttecht, V. Kao, and O. Agrawal, "Chalcogenide glass bistable resistivity (Ovonic) memories," *IEEE Trans. Magn.*, vol. 6, no. 3, pp. 592–592, Sep. 1970.

[76] M. Wuttig and N. Yamada, "Phase-change materials for rewriteable data storage," *Nature Mater.*, vol. 6, pp. 824–832, 2007.

[77] T. Oka and N. Nagaosa, "Interfaces of correlated electron systems: Proposed mechanism for colossal electroresistance," *Phys. Rev. Lett.*, vol. 95, 2005, Art. ID. 266403.

[78] R. Fors, S. I. Khartsev, and A. M. Grishin, "Giant resistance switching in metal-insulator-manganite junctions: Evidence for Mott transition," *Phys. Rev. B*, vol. 71, 2005, Art. ID. 045305.

[79] P. P. Boriskov, A. A. Velichko, A. L. Pergament, G. B. Stefanovich, and D. G. Stefanovich, "The effect of electric field on metal-insulator phase transition in vanadium dioxide," *Tech. Phys. Lett.*, vol. 28, pp. 406–408, 2002.

[80] C. Ko and S. Ramanathan, "Observation of electric field-assisted phase transition in thin film vanadium oxide in a metal-oxide-semiconductor device geometry," *Appl. Phys. Lett.*, vol. 93, 2008, Art. ID. 252101.

[81] G. Stefanovich, A. Pergament, and D. Stefanovich, "Electrical switching and Mott transition in VO_2," *J. Phys., Condensed Matter*, vol. 12, pp. 8837–8845, 2000.

[82] P. Stoliar *et al.*, "Universal electric-field-driven resistive transition in narrow-gap Mott insulators," *Adv. Mater.*, vol. 25, pp. 3222–3226, 2013.

[83] F. Nakamura *et al.*, "Electric-field-induced metal maintained by current of the Mott insulator Ca_2RuO_4," *Sci. Rep.*, vol. 3, 2013, Art. ID. 2536.

[84] A. Zimmers *et al.*, "Role of thermal heating on the voltage induced insulator-metal transition in VO_2," *Phys. Rev. Lett.*, vol. 110, 2013, Art. ID. 056601.

[85] X. Zhong, X. Zhang, A. Gupta, and P. LeClair, "Avalanche breakdown in microscale VO_2 structures," *J. Appl. Phys.*, vol. 110, 2011, Art. ID. 084516.

[86] G. Gopalakrishnan, D. Ruzmetov, and S. Ramanathan, "On the triggering mechanism for the metal-insulator transition in thin film VO_2 devices: Electric field versus thermal effects," *J. Mater. Sci.*, vol. 44, pp. 5345–5353, 2009.

[87] B. S. Mun *et al.*, "Role of joule heating effect and bulk-surface phases in voltage-driven metal-insulator transition in VO_2 crystal," *Appl. Phys. Lett.*, vol. 103, 2013, Art. ID. 061902.

[88] B. Fisher, J. Genossar, K. B. Chashka, L. Patlagan, and G. M. Reisner, "Metal-insulator transition upon heating and negative-differential-resistive-switching induced by self-heating in $BaCo_{0.9}Ni_{0.1}S_{1.8}$," *Appl. Phys. Lett.*, vol. 104, 2014, Art. ID. 153511.

[89] L. Cario, C. Vaju, B. Corraze, V. Guiot, and E. Janod, "Electric-field-induced resistive switching in a family of Mott insulators: Towards a new class of RRAM memories," *Adv. Mater.*, vol. 22, pp. 5193–5197, 2010.

[90] P. Stoliar *et al.*, "Universal electric-field-driven resistive transition in narrow-gap Mott insulators," *Adv. Mater.*, vol. 25, pp. 3222–3226, 2013.

[91] V. Dubost *et al.*, "Resistive switching at the nanoscale in the Mott insulator compound $GaTa_4Se_8$," *Nano Lett.*, vol. 13, pp. 3648–3653, 2013.

[92] Y. Zhou and S. Ramanathan, "Correlated electron materials and field effect transistors for logic: A review," *Critical Rev. Solid State Mater. Sci.*, vol. 38, pp. 286–317, 2013.

[93] K. Hyun-Tak *et al.*, "Mechanism and observation of Mott transition in VO_2-based two- and three-terminal devices," *New J. Phys.*, vol. 6, 2004, Art. ID. 52.

[94] S. Sengupta *et al.*, "Field-effect modulation of conductance in VO_2 nanobeam transistors withHfO_2 as the gate dielectric," *Appl. Phys. Lett.*, vol. 99, 2011, Art. ID. 062114.

[95] D. M. Newns *et al.*, "Mott transition field effect transistor," *Appl. Phys. Lett.*, vol. 73, pp. 780–782, 1998.

[96] C. H. Ahn *et al.*, "Electrostatic modification of novel materials," *Rev. Modern Phys.*, vol. 78, pp. 1185–1212, 2006.

[97] H. Takagi and H. Y. Hwang, "An emergent change of phase for electronics," *Science*, vol. 327, pp. 1601–1602, 2010.

[98] M. Galiński, A. Lewandowski, and I. Stępniak, "Ionic liquids as electrolytes,"

Electrochimica Acta, vol. 51, pp. 5567–5580, 2006.

[99] T. Fujimoto and K. Awaga, "Electric-double-layer field-effect transistors with ionic liquids," *Phys. Chem. Chem. Phys.*, vol. 15, pp. 8983–9006, 2013.

[100] P. Moetakef *et al.*, "Electrostatic carrier doping of GdTiO3/SrTiO3 interfaces," *Appl. Phys. Lett.*, vol. 99, 2011, Art. ID. 232116.

[101] Y. Lee *et al.*, "Phase diagram of electrostatically doped $SrTiO_3$," *Phys. Rev. Lett.*, vol. 106, 2011, Art. ID. 136809.

[102] Z. Yang, Y. Zhou, and S. Ramanathan, "Studies on room-temperature electric-field effect in ionic-liquid gated VO_2 three-terminal devices," *J. Appl. Phys.*, vol. 111, 2012, Art. ID. 014506.

[103] M. Nakano *et al.*, "Collective bulk carrier delocalization driven by electrostatic surface charge accumulation," *Nature*, vol. 487, pp. 459–462, 2012.

[104] K. Liu *et al.*, "Dense electron system from gate-controlled surface metal-insulator transition," *Nano Lett.*, vol. 12, pp. 6272–6277, 2012.

[105] Y. Zhou and S. Ramanathan, "Relaxation dynamics of ionic liquid—VO_2 interfaces and influence in electric double-layer transistors," *J. Appl. Phys.*, vol. 111, 2012, Art. ID. 084508.

[106] H. Ji, J. Wei, and D. Natelson, "Modulation of the electrical properties of VO_2 nanobeams using an ionic liquid as a gating medium," *Nano Lett.*, vol. 12, pp. 2988–2992, 2012.

[107] J. Lu, K. G. West, and S. A. Wolf, "Very large anisotropy in the dc conductivity of epitaxial VO_2 thin films grown on (011) rutile TiO_2 substrates," *Appl. Phys. Lett.*, vol. 93, 2008, Art. ID. 262107.

[108] A. Gupta *et al.*, "Semiconductor to metal transition characteristics of VO_2 thin films grown epitaxially on Si (001)," *Appl. Phys. Lett.*, vol. 95, 2009, Art. ID. 111915.

[109] Y. Zhou and S. Ramanathan, "Heteroepitaxial VO_2 thin films on GaN: Structure and metal-insulator transition characteristics," *J. Appl. Phys.*, vol. 112, 2012, Art. ID. 074114.

[110] D. Ruzmetov, K. T. Zawilski, V. Narayanamurti, and S. Ramanathan, "Structure-functional property relationships in rf-sputtered vanadium dioxide thin films," *J. Appl. Phys.*, vol. 102, 2007, Art. ID. 113715.

[111] D. H. Kim and H. S. Kwok, "Pulsed laser deposition of VO_2 thin films," *Appl. Phys. Lett.*, vol. 65, pp. 3188–3190, 1994.

[112] R. Scherwitzl *et al.*, "Electric-field control of the metal-insulator transition in ultrathinNdNiO_3 films," *Adv. Mater.*, vol. 22, pp. 5517–5520, 2010.

[113] C. A. F. Vaz, J. A. Moyer, D. A. Arena, C. H. Ahn, and V. E. Henrich, "Magnetic and electronic structure of ultrathin $La_{1-x}Sr_xMnO_3$ films at half doping," *Phys. Rev. B*, vol. 90, 2014, Art. ID. 024414.

[114] P. J. Hood and J. F. DeNatale, "Millimeter-wave dielectric properties of epitaxial vanadium dioxide thin films," *J. Appl. Phys.*, vol. 70, pp. 376–381, 1991.

[115] G. Rampelberg *et al.*, "Semiconductor-metal transition in thinVO_2 films grown by ozone based atomic layer deposition," *Appl. Phys. Lett.*, vol. 98, 2011, Art. ID. 162902.

[116] T. Blanquart *et al.*, "Atomic layer deposition and characterization of vanadium oxide thin films," *RSC Adv.*, vol. 3, pp. 1179–1185, 2013.

[117] M. B. Sahana, G. N. Subbanna, and S. A. Shivashankar, "Phase transformation and semiconductor-metal transition in thin films ofVO_2 deposited by low-pressure metalorganic chemical vapor deposition," *J. Appl. Phys.*, vol. 92, pp. 6495–6504, 2002.

[118] T. Maruyama and Y. Ikuta, "Vanadium dioxide thin films prepared by chemical vapour deposition from vanadium(III) acetylacetonate," *J. Mater. Sci.*, vol. 28, pp. 5073–5078, 1993.

[119] P. Moetakef, J. Y. Zhang, S. Raghavan, A. P. Kajdos, and S. Stemmer, "Growth window and effect of substrate symmetry in hybrid molecular beam epitaxy of a Mott insulating rare earth titanate," *J. Vacuum Sci. Technol. A*, vol. 31, 2013, Art. ID. 041503.

[120] J. W. Tashman *et al.*, "Epitaxial growth of VO_2 by periodic annealing," *Appl. Phys. Lett.*, vol. 104, 2014, Art. ID. 063104.

[121] B.-G. Chae *et al.*, "Highly oriented VO_2 thin films prepared by sol-gel deposition," *Electrochem. Solid-State Lett.*, vol. 9, pp. C12–C14, 2006.

[122] C. Cen *et al.*, "Nanoscale control of an interfacial metal-insulator transition at room temperature," *Nature Mater.*, vol. 7, pp. 298–302, 2008.

[123] T. Kimura *et al.*, "Magnetic control of ferroelectric polarization," *Nature*, vol. 426, pp. 55–58, 2003.

[124] A. Urushibara *et al.*, "Insulator-metal transition and giant magnetoresistance in $La_{1-x}Sr_xMnO_3$," *Phys. Rev. B*, vol. 51, pp. 14103–14109, 1995.

[125] H. H. Y. X. Yan-Wu, "Tuning the electrons at the $LaAlO_3/SrTiO_3$ interface: From growth to beyond growth," *Chin. Phys. B*, vol. 22, 2013, Art. ID. 127301.

[126] R. Lopez, T. E. Haynes, L. A. Boatner, L. C. Feldman, and R. F. Haglund, "Size effects in the structural phase transition of VO_2 nanoparticles," *Phys. Rev. B*, vol. 65, 2002, Art. ID. 224113.

[127] J. Wu *et al.*, "Strain-induced self organization of metal-insulator domains in single-crystalline VO_2 nanobeams," *Nano Lett.*, vol. 6, pp. 2313–2317, 2006.

[128] S. Zhang, J. Y. Chou, and L. J. Lauhon, "Direct correlation of structural domain formation with the metal insulator transition in a VO_2 nanobeam," *Nano Lett.*, vol. 9, pp. 4527–4532, 2009.

[129] J. I. Sohn *et al.*, "Direct observation of the structural component of the metal-insulator phase transition and growth habits of epitaxially grown VO_2 nanowires," *Nano Lett.*, vol. 7, pp. 1570–1574, 2007.

[130] J. M. Baik, M. H. Kim, C. Larson, A. M. Wodtke, and M. Moskovits, "Nanostructure-dependent metal-insulator transitions in vanadium-oxide nanowires," *J. Phys. Chem. C*, vol. 112, pp. 13 328–13 331, 2008.

[131] R. Jaramillo, F. Schoofs, S. D. Ha, and S. Ramanathan, "High pressure synthesis of $SmNiO_3$ thin films and implications for thermodynamics of the nickelates," *J. Mater. Chem. C*, vol. 1, pp. 2455–2462, 2013.

[132] J. Shi, Y. Zhou, and S. Ramanathan, "Colossal resistance switching and band gap modulation in a perovskite nickelate by electron doping," *Nature Commun.*, vol. 5, 2014, Art. ID. 5860.

[133] G. W. Burr *et al.*, "Access devices for 3D crosspoint memorya)," *J. Vacuum Sci. Technol. B*, vol. 32, 2014, Art. ID. 040802.

[134] M. J. Lee *et al.*, "Two series oxide resistors applicable to high speed and high density nonvolatile memory," *Adv. Mater.*, vol. 19, pp. 3919–3923, 2007.

[135] I. P. Radu *et al.*, "Vanadium dioxide for selector applications," *ECS Trans.*, vol. 58, pp. 249–258, 2013.

[136] K. Martens *et al.*, "The VO_2 interface, the metal-insulator transition tunnel junction, and the metal-insulator transition switch on-off resistance," *J. Appl. Phys.*, vol. 112, 2012, Art. ID. 124501.

[137] X. Liu *et al.*, "Co-occurrence of threshold switching and memory switching in Pt/NbO_x/Pt cells for crosspoint memory applications," *IEEE Electron Device Lett.*, vol. 33, no. 2, pp. 236–238, Feb. 2012.

[138] S. Kim, W. Lee, and H. Hwang, "Selector devices for cross-point ReRAM," in *Proc. 13th Int. Workshop Cellular Nanoscale Netw. Their Appl.*, 2012, DOI: 10.1109/CNNA.2012.6331466.

[139] E. Cha *et al.*, "Nanoscale 10 nm 3D vertical ReRAM andNbO_2 threshold selector with TiN electrode," in *Proc. IEEE Int. Electron Devices Meeting*, 2013, pp. 10.5.1–10.5.4.

[140] X. Liu *et al.*, "Reduced threshold current in NbO_2 selector by engineering device structure," *IEEE Electron Device Lett.*, vol. 35, no. 10, pp. 1055–1057, Oct. 2014.

[141] X. Liu *et al.*, "Complementary resistive switching in niobium oxide-based resistive memory devices," *IEEE Electron Device Lett.*, vol. 34, no. 2, pp. 235–237, Feb. 2013.

[142] M. Son *et al.*, "Self-selective characteristics of nanoscale devices for high-density ReRAM applications," *IEEE Electron Device Lett.*, vol. 33, no. 5, pp. 718–720, May 2012.

[143] M. Son *et al.*, "Excellent selector characteristics of nanoscale for high-density bipolar ReRAM applications," *IEEE Electron Device Lett.*, vol. 32, no. 11, pp. 1579–1581, Nov. 2011.

[144] S. Kim *et al.*, "Ultrathin < 10 nm Nb_2O_5/NbO_2 hybrid memory with both memory and selector characteristics for high density 3D vertically stackable RRAM applications," in *Proc. Symp. VLSI Technol.*, 2012, pp. 155–156.

[145] H.-S. Wong *et al.*, "Metal-oxide RRAM," *Proc. IEEE*, vol. 100, no. 6, pp. 1951–1970, Jun. 2012.

[146] K. M. Kim, D. S. Jeong, and C. S. Hwang, "Nanofilamentary resistive switching in binary oxide system; A review on the present status and outlook," *Nanotechnology*, vol. 22, 2011, Art. ID. 254002.

[147] I. G. Baek *et al.*, "Highly scalable nonvolatile resistive memory using simple binary oxide driven by asymmetric unipolar voltage pulses," in *IEDM Tech. Dig. IEEE Int. Electron Devices Meeting*, 2004, pp. 587–590.

[148] K. Tsunoda *et al.*, "Low power and high speed switching of Ti-doped NiO ReRAM under the unipolar voltage source of less than 3 V," in *Proc. IEEE Int. Electron Devices Meeting*, 2007, pp. 767–770.

[149] L. F. Liu *et al.*, "Current compliance-free resistive switching in nonstoichiometric CeO_x films for nonvolatile memory application," in *Proc. IEEE Int. Memory Workshop*, 2009, DOI: 10.1109/IMW.2009.5090586.

[150] H. B. Lv *et al.*, "Resistive memory switching of Cu_xO films for a nonvolatile

memory application," *IEEE Electron Device Lett.*, vol. 29, no. 4, pp. 309–311, Apr. 2008.

[151] K. Sungho, M. Hanul, D. Gupta, Y. Seunghyup, and Y.-K. Choi, "Resistive switching characteristics of sol-gel zinc oxide films for flexible memory applications," *IEEE Trans. Electron Devices*, vol. 56, no. 4, pp. 696–699, Apr. 2009.

[152] H. Y. Lee *et al.*, "Low power and high speed bipolar switching with a thin reactive Ti buffer layer in robust HfO_2 based RRAM," in *Proc. IEEE Int. Electron Devices Meeting*, 2008, DOI: 10.1109/IEDM.2008.4796677.

[153] S. Seo *et al.*, "Reproducible resistance switching in polycrystalline NiO films," *Appl. Phys. Lett.*, vol. 85, pp. 5655–5657, 2004.

[154] T. Sakata, K. Sakata, G. Höfer, and T. Horiuchi, "Preparation of NbO_2 single crystals by chemical transport reaction," *J. Crystal Growth*, vol. 12, pp. 88–92, 1972.

[155] S. D. Ha, Z. You, A. E. Duwel, D. W. White, and S. Ramanathan, "Quick switch: Strongly correlated electronic phase transition systems for cutting-edge microwave devices," *IEEE Microw. Mag.*, vol. 15, no. 6, pp. 32–44, Sep./Oct. 2014.

[156] M. D. Pickett, J. Borghetti, J. J. Yang, G. Medeiros-Ribeiro, and R. S. Williams, "Coexistence of memristance and negative differential resistance in a nanoscale metal-oxide-metal system," *Adv. Mater.*, vol. 23, pp. 1730–1733, 2011.

[157] M. Son *et al.*, "Self-selective characteristics of nanoscale VO_x devices for high-density ReRAM applications," *IEEE Electron Device Lett.*, vol. 33, no. 5, pp. 718–720, May 2012.

[158] A. S. Barker, H. W. Verleur, and H. J. Guggenheim, "Infrared optical properties of vanadium dioxide above and below the transition temperature," *Phys. Rev. Lett.*, vol. 17, pp. 1286–1289, 1966.

[159] A. Zylbersztejn, B. Pannetier, and P. Merenda, "Fast pulse measurements of the dielectric constant of semiconducting VO_2," *Phys. Lett. A*, vol. 54, pp. 145–147, 1975.

[160] Z. Yang, C. Ko, V. Balakrishnan, G. Gopalakrishnan, and S. Ramanathan, "Dielectric and carrier transport properties of vanadium dioxide thin films across the phase transition utilizing gated capacitor devices," *Phys. Rev. B*, vol. 82, 2010, Art. ID. 205101.

[161] M. Kim *et al.*, "A new single element phase transition memory," in *Proc. 10th IEEE Conf. Nanotechnol.*, 2010, pp. 439–442.

[162] S. H. Lee *et al.*, "Vanadium dioxide (VO_2) is also a ferroelectric: Properties from memory structures," in *Proc. 11th IEEE Conf. Nanotechnol.*, 2011, pp. 735–739.

[163] H. Sang *et al.*, "Space charge polarization induced memory in $SmNiO_3$/Si transistors," *Appl. Phys. Lett.*, vol. 102, 2013, Art. ID. 072102.

[164] T. Driscoll, H.-T. Kim, B.-G. Chae, M. Di Ventra, and D. N. Basov, "Phase-transition driven memristive system," *Appl. Phys. Lett.*, vol. 95, 2009, Art. ID. 043503.

[165] T. Driscoll *et al.*, "Memory metamaterials," *Science*, vol. 325, pp. 1518–1521, 2009.

[166] Y.-G. Jeong *et al.*, "Electrical control of terahertz nano antennas on VO_2 thin film," *Opt. Exp.*, vol. 19, pp. 21 211–21 215, 2011.

[167] D. J. Shelton, K. R. Coffey, and G. D. Boreman, "Experimental demonstration of tunable phase in a thermochromic infrared-reflectarray metamaterial," *Opt. Exp.*, vol. 18, pp. 1330–1335, 2010.

[168] M. J. Dicken *et al.*, "Frequency tunable near-infrared metamaterials based on VO_2 phase transition," *Opt. Exp.*, vol. 17, pp. 18 330–18 339, 2009.

[169] A. K. Jain, J. Mao, and K. Mohiuddin, "Artificial neural networks: A tutorial," *Computer*, vol. 29, pp. 31–44, 1996.

[170] IBM Blue Gene Team, "Overview of the IBM Blue Gene/P project," *IBM J. Res. Develop.*, vol. 52, pp. 199–220, 2008.

[171] Q. V. Le, "Building high-level features using large scale unsupervised learning," in *Proc. IEEE Int. Conf. Acoust. Speech Signal Process.*, 2013, pp. 8595–8598.

[172] R. Ananthanarayanan, S. K. Esser, H. D. Simon, and D. S. Modha, "The cat is out of the bag: Cortical simulations with 109 neurons, 1013 synapses," in *Proc. Conf. High Performance Comput. Netw. Storage Anal.*, 2009, DOI: 10.1145/1654059.1654124.

[173] K. Minkovich, N. Srinivasa, J. M. Cruz-Albrecht, C. Youngkwan, and A. Nogin, "Programming time-multiplexed reconfigurable hardware using a scalable neuromorphic compiler," *IEEE Trans. Neural Netw. Learn. Syst.*, vol. 23, no. 6, pp. 889–901, Jun. 2012.

[174] P. A. Merolla *et al.*, "A million spiking-neuron integrated circuit with a scalable communication network and interface," *Science*, vol. 345, pp. 668–673, 2014.

[175] D. Kuzum, S. Yu, and H. S. P. Wong, "Synaptic electronics: Materials, devices and applications," *Nanotechnology*, vol. 24, 2013, Art. ID. 382001.

[176] T. Sharp, F. Galluppi, A. Rast, and S. Furber, "Power-efficient simulation of detailed cortical microcircuits on SpiNNaker," *J. Neurosci. Methods*, vol. 210, pp. 110–118, 2012.

[177] K.-H. Kim *et al.*, "A functional hybrid memristor crossbar-array/CMOS system for data storage and neuromorphic applications," *Nano Lett.*, vol. 12, pp. 389–395, 2012.

[178] A. L. Hodgkin and A. F. Huxley, "A quantitative description of membrane current and its application to conduction and excitation in nerve," *J. Physiol.*, vol. 117, pp. 500–544, 1952.

[179] M. D. Pickett, G. Medeiros-Ribeiro, and R. S. Williams, "A scalable neuristor built with Mott memristors," *Nature Mater.*, vol. 12, pp. 114–117, 2013.

[180] J. Nagumo, S. Arimoto, and S. Yoshizawa, "An active pulse transmission line simulating nerve axon," *Proc. IRE*, vol. 50, pp. 2061–2070, 1962.

[181] J.-I. Nishizawa and A. Hayasaka, "Two-line neuristor with active element in series and in parallel†," *Int. J. Electron.*, vol. 26, pp. 437–469, 1969.

[182] H. Markram, J. Lübke, M. Frotscher, and B. Sakmann, "Regulation of synaptic efficacy by coincidence of postsynaptic APs and EPSPs," *Science*, vol. 275, pp. 213–215, 1997.

[183] G.-Q. Bi and M.-M. Poo, "Synaptic modifications in cultured hippocampal neurons: Dependence on spike timing, synaptic strength, and postsynaptic cell type," *J. Neurosci.*, vol. 18, pp. 10 464–10 472, 1998.

[184] F. Alibart, E. Zamanidoost, and D. B. Strukov, "Pattern classification by memristive crossbar circuits using *ex situ* and *in situ* training," *Nature Commun.*, vol. 4, 2013, Art. ID. 2032.

[185] C. Diorio, P. Hasler, B. A. Minch, and C. A. Mead, "A single-transistor silicon synapse," *IEEE Trans. Electron Devices*, vol. 43, no. 11, pp. 1972–1980, Nov. 1996.

[186] J. Shi, S. D. Ha, Y. Zhou, F. Schoofs, and S. Ramanathan, "A correlated nickelate synaptic transistor," *Nature Commun.*, vol. 4, 2013, Art. ID. 3676.

[187] S. D. Ha, J. Shi, Y. Meroz, L. Mahadevan, and S. Ramanathan, "Neuromimetic circuits with synaptic devices based on strongly correlated electron systems," *Phys. Rev. Appl.*, vol. 2, 2014, Art. ID. 064003.

[188] D. Loke *et al.*, "Breaking the speed limits of phase-change memory," *Science*, vol. 336, pp. 1566–1569, 2012.

[189] M. Rini *et al.*, "Control of the electronic phase of a manganite by mode-selective vibrational excitation," *Nature*, vol. 449, pp. 72–74, 2007.

[190] M. K. Liu *et al.*, "Photoinduced phase transitions by time-resolved far-infrared spectroscopy in VO_2," *Phys. Rev. Lett.*, vol. 107, 2011, Art. ID. 066403.

[191] M. F. Becker *et al.*, "Femtosecond laser excitation of the semiconductor-metal phase transition inVO_2," *Appl. Phys. Lett.*, vol. 65, pp. 1507–1509, 1994.

[192] L. A. Gea and L. A. Boatner, "Optical switching of coherent VO_2 precipitates formed in sapphire by ion implantation and annealing," *Appl. Phys. Lett.*, vol. 68, pp. 3081–3083, 1996.

[193] C. Kübler *et al.*, "Coherent structural dynamics and electronic correlations during an ultrafast insulator-to-metal phase transition in VO_2," *Phys. Rev. Lett.*, vol. 99, 2007, Art. ID. 116401.

[194] M. Nakajima, N. Takubo, Z. Hiroi, Y. Ueda, and T. Suemoto, "Photoinduced metallic state in VO_2 proved by the terahertz pump-probe spectroscopy," *Appl. Phys. Lett.*, vol. 92, 2008, Art. ID. 011907.

[195] H.-T. Kim *et al.*, "Monoclinic and correlated metal phase in VO_2 as evidence of the Mott transition: Coherent phonon analysis," *Phys. Rev. Lett.*, vol. 97, 2006, Art. ID. 266401.

[196] M. Liu *et al.*, "Terahertz-field-induced insulator-to-metal transition in vanadium dioxide metamaterial," *Nature*, vol. 487, pp. 345–348, 2012.

[197] K. Appavoo *et al.*, "Ultrafast phase transition via catastrophic phonon collapse driven by plasmonic hot-electron injection," *Nano Lett.*, vol. 14, pp. 1127–1133, 2014.

[198] S. Lysenko *et al.*, "Light-induced ultrafast phase transitions in VO_2 thin film," *Appl. Surface Sci.*, vol. 252, pp. 5512–5515, 2006.

[199] S. Lysenko, A. Rúa, V. Vikhnin, F. Fernández, and H. Liu, "Insulator-to-metal phase transition and recovery processes in VO_2 thin films after femtosecond laser excitation," *Phys. Rev. B*, vol. 76, 2007, Art. ID. 035104.

[200] M. Liu *et al.*, "Terahertz-field-induced insulator-to-metal transition in vanadium dioxide metamaterial," *Nature*, vol. 487, pp. 345–348, 2012.

[201] L. Perfetti *et al.*, "Time evolution of the electronic structure of 1T-TaS_2 through the insulator-metal transition," *Phys. Rev. Lett.*, vol. 97, 2006, Art. ID. 067402.

[202] B.-G. Chae, H.-T. Kim, D.-H. Youn, and K.-Y. Kang, "Abrupt metal-insulator

transition observed in VO_2 thin films induced by a switching voltage pulse," *Physica B, Condensed Matter*, vol. 369, pp. 76–80, 2005.

[203] R. Servin *et al.*, "Unravelling the switching mechanisms in electric field induced insulator-metal transitions in VO_2 nanobeams," *J. Phys. D, Appl. Phys.*, vol. 47, 2014, Art. ID. 295101.

[204] J. S. Brockman *et al.*, "Subnanosecond incubation times for electric-field-induced metallization of a correlated electron oxide," *Nature Nanotechnol.*, vol. 9, pp. 453–458, 2014.

[205] G. Seo *et al.*, "Voltage-pulse-induced switching dynamics in VO_2 thin-film devices on silicon," *IEEE Electron Device Lett.*, vol. 32, no. 11, pp. 1582–1584, Nov. 2011.

[206] A. Kar *et al.*, "Intrinsic electronic switching time in ultrathin epitaxial vanadium dioxide thin film," *Appl. Phys. Lett.*, vol. 102, 2013, Art. ID. 072106.

[207] Y. Zhang and S. Ramanathan, "Analysis of "on" and "off" times for thermally driven VO_2 metal-insulator transition nanoscale switching devices," *Solid-State Electron.*, vol. 62, pp. 161–164, 2011.

[208] S. Hormoz and S. Ramanathan, "Limits on vanadium oxide Mott metal-insulator transition field-effect transistors," *Solid-State Electron.*, vol. 54, pp. 654–659, 2010.

[209] K. T. Jacob, C. Shekhar, M. Vinay, and Y. Waseda, "Thermodynamic properties of niobium oxides," *J. Chem. Eng. Data*, vol. 55, pp. 4854–4863, 2010.

[210] C. N. Berglund and H. J. Guggenheim, "Electronic properties of VO_2 near the semiconductor-metal transition," *Phys. Rev.*, vol. 185, pp. 1022–1033, 1969.

[211] D.-W. Oh, C. Ko, S. Ramanathan, and D. G. Cahill, "Thermal conductivity and dynamic heat capacity across the metal-insulator transition in thin film VO_2," *Appl. Phys. Lett.*, vol. 96, 2010, Art. ID. 151906.

ABOUT THE AUTHORS

You Zhou received the B.S. degree in physics from Peking University, Beijing, China, in 2010 and the Ph.D. degree in applied physics from Harvard University, Cambridge, MA, USA, in 2015.

He is currently a Postdoctoral Fellow in the John A. Paulson School of Engineering and Applied Sciences, Harvard University. His research has focused on the material physics of complex oxides and their applications to electronic and optical devices as well as energy conversion.

Shriram Ramanathan received the Ph.D. degree in materials science and engineering from Stanford University, Stanford, CA, USA, in 2002. His doctoral dissertation was carried out under the supervision of P. C. McIntyre.

He subsequently joined the research staff at Components Research, Intel, and worked on realization of 3-D integrated circuits and high-resolution noninvasive microscope design for over three years. He has since served on the Applied Physics faculty at Harvard University, Cambridge, MA, USA. His research interests are in the areas of thin-film oxide materials science and solid-state devices.